SINGLE PARTICLE COMBUSTION ANALYSIS OF BIOMASS FUELS BY USING WIRE MESH REACTOR

A THESIS SUBMITTED TO
THE GRADUATE SCHOOL OF NATURAL AND APPLIED SCIENCES
OF
MIDDLE EAST TECHNICAL UNIVERSITY

BY

KAAN GÜREL

IN PARTIAL FULFILLMENT OF THE REQUIREMENTS
FOR
THE DEGREE OF MASTER OF SCIENCE
IN
MECHANICAL ENGINEERING

JULY 2021

Approval of the thesis:

SINGLE PARTICLE COMBUSTION ANALYSIS OF BIOMASS FUELS BY USING WIRE MESH REACTOR

submitted by **KAAN GÜREL** in partial fulfillment of the requirements for the degree of **Master of Science** i**n Mechanical Engineering, Middle East Technical University** by,

Prof. Dr. Halil Kalıpçılar
Dean, Graduate School of **Natural and Applied Sciences** _____

Prof. Dr. Mehmet Ali Sahir Arıkan
Head of the Department, **Mechanical Engineering** _____

Assoc. Prof. Dr. Feyza Kazanç Özerinç
Supervisor, **Mechanical Engineering, METU** _____

Examining Committee Members:

Prof. Dr. İlker Tarı
Mechanical Engineering, METU _____

Assoc. Prof. Dr. Feyza Kazanç Özerinç
Mechanical Engineering, METU _____

Prof. Dr. Ahmet Yozgatlıgil
Mechanical Engineering, METU _____

Assoc. Prof. Dr. Onur Taylan
Mechanical Engineering, METU _____

Assoc. Prof. Dr. Zeki Yılmazoğlu
Mechanical Engineering, Gazi University _____

Date: 30.07.2021

I hereby declare that all information in this document has been obtained and presented in accordance with academic rules and ethical conduct. I also declare that, as required by these rules and conduct, I have fully cited and referenced all material and results that are not original to this work.

Name Last name : Kaan Gürel

Signature :

ABSTRACT

SINGLE PARTICLE COMBUSTION ANALYSIS OF BIOMASS FUELS BY USING WIRE MESH REACTOR

Gürel, Kaan
Master of Science, Mechanical Engineering
Supervisor: Assoc. Prof. Dr. Feyza Kazanç Özerinç

July 2021, 76 pages

This thesis investigates the single particle combustion behavior of a Turkish lignite and two agricultural biomass fuels using a recently developed wire mesh reactor coupled with a high-speed camera. The fuels under investigation are endogenous of Turkey and present potential to gradually replace the currently burned lignite coals for electricity generation. This change requires a large amount of data so that the oftentimes disparate fuels can be properly co-fired. The scientific outcome of the study will be understanding the influence of fuel type, particle size and mass, and thermal pre-treatment on parameters such as the ignition delay time and burnout time which are of extreme importance for co-firing purposes. The wire mesh reactor to be used enables conditions that resemble those found in large scale combustion systems (i.e., high temperatures and high heating rates). The fuel particles with different masses were heated to 1000 ºC by radiation with a heating rate of 900ºC/s. To understand the effects of thermal pre-treatment, fuels are torrefied, slow and fast pyrolyzed. The time analysis demonstrated that the particle mass and size did not affect ignition delay time; however, slow pyrolysis had a significant effect on the ignition delay time. The ignition delay time was tremendously increased for the chars produced from slow pyrolysis (~10 s) compared to raw (~3 s) and other heat-treated

particles (~4 s) for all fuels. Burnout times of all fuels increased proportionally with particle mass. Fast and slow pyrolysis generally increased the char combustion and burnout times. The average burnout times for chars from fast and slow pyrolysis of biomass was ~20 s and ~29 s, respectively, while those of raw biomass was ~9 s. The average burnout times for chars from fast and slow pyrolysis of lignite was ~20 s and ~53 s, respectively, while those of raw lignite was ~19 s, when 2 mg particles were compared. Chars from fast pyrolysis of both biomasses had similar burnout times (~20 s) compared to the that of raw Tunçbilek Lignite (~19 s). This depicts the potential of co-firing TL with biomass chars produced from fast pyrolysis.

Keywords: Singe Particle, Pyrolysis, Torrefaction, Biomass, Wire Mesh Reactor

ÖZ

TEL ÖRGÜ REAKTÖRÜ KULLANARAK BİYOKÜTLE YAKITLARIN TEK PARÇACIK YANMA ANALİZİ

Gürel, Kaan
Yüksek Lisans, Makina Mühendisliği
Tez Yöneticisi: Doç. Dr. Feyza Kazanç Özerinç

Temmuz 2021, 76 sayfa

Bu tez, yüksek hızlı bir kamera ile birleştirilmiş yeni geliştirilen bir tel örgü reaktörü kullanarak birkaç biyokütle yakıtının tek parçacık yanma davranışını araştırıyor. İncelenmekte olan yakıtlar Türkiye'ye özgüdür ve halihazırda yakılan linyit kömürlerini elektrik üretimi için aşamalı olarak değiştirme potansiyeli sunmaktadır. Bu değişiklik, büyük ölçüde veri gerektirir; böylece, zaman zaman bağımsız yakıtlar, uygun şekilde birlikte ateşlenebilir. Çalışmanın bilimsel sonucu, yakıt türü, partikül büyüklüğü ve termal ön işlemin, ateşleme gecikme süresi ve yanma süresi gibi birlikte ateşleme amaçları için çok önemli olan parametreler üzerindeki etkisi olacaktır. Kullanılacak tel örgü reaktörü, büyük ölçekli yanma sistemlerinde bulunanlara (örneğin, yüksek sıcaklıklar ve yüksek ısıtma hızları) benzeyen koşulları sağlar. Farklı kütlelere sahip yakıt partikülleri, 900ºC/s ısıtma hızıyla radyasyonla 1000 ºC'ye ısıtıldı. Termal ön işlemin etkilerini anlamak için yakıtlar kavruldu, yavaş ve hızlı bir şekilde piroliz edildi. Zaman analizi, partikül kütlesinin ve boyutunun tutuşma gecikme süresini etkilemediğini göstermiştir; fakat, yavaş piroliz, tutuşma gecikme süresi üzerinde önemli bir etkiye sahipti. Yavaş pirolizden (~10 s) üretilen çarlar için tutuşma gecikme süresi, ham (~3 s) ve diğer ısıl işlem görmüş partiküllere (~4 s) kıyasla, tüm yakıtlar icin muazzam derecede artmıştır. Tüm yakıtların yanma

süreleri partikül kütlesi ile orantılı olarak artmıştır. Hızlı ve yavaş piroliz genellikle çar yanmasını ve yanma sürelerini artırmıştır. Biyokütlenin hızlı ve yavaş pirolizinden oluşan çarların ortalama tükenme süreleri sırasıyla ~20 s ve ~29 s iken, ham biyokütleninki ~9 s idi. 2 mg partiküller karşılaştırıldığında, linyitin hızlı ve yavaş pirolizinden oluşan çarların ortalama yanma süreleri sırasıyla ~20 s ve ~53 s iken, ham linyitinki ~19 s idi. Her iki biyokütlenin hızlı pirolizinden elde edilen çarlar, ham linyit (~19 s) ile karşılaştırıldığında benzer tükenme sürelerine (~20 s) sahipti. Bu, linyitin hızlı pirolizden üretilen biyokütle çarları ile birlikte yakma potansiyelini göstermektedir.

Anahtar Kelimeler: Tek Parçacık, Piroliz, Kavurma, Biyokütle, Tel Örgü Reaktörü

To my family and loved ones

ACKNOWLEDGMENTS

I would like to express my deepest gratitude to my supervisor Assoc. Prof. Dr. Feyza Kazanç Özerinç for her guidance, advice, criticism, encouragements, insight, and most importantly, her friendship and understanding throughout my five years of time in the Clean Combustion Technologies Laboratory and the long way up to getting my master's degree. This work would not happen without her support and encouragement.

I would like to thank Dr. Duarte Magalhaes for his help throughout my working days in the laboratory. His mentorship and friendship broadened my point of view towards the life. Also, I would like to express my gratitude to my laboratory collages Alican Akgül, Süleyman Şener Akın, Burak Özer, and Mammadbaghir Baghirzade for their support, assistance and their friendship during all this five years.

I would also like to thank Prof. Altan Kayran from Department of Aerospace Engineering for allowing us to do the preliminary analysis on TGA experimental setup in his laboratory at RUZGEM of the Middle East Technical University. For the support on the preliminary analysis, I would like to thank Central Laboratory of the Middle East Technical University.

I gratefully acknowledge financial support from the Royal Society Advanced Newton Fellowship (grant number NA140020).

I would like to show my greatest appreciation towards my family for their constant support throughout my educational life.

And finally, I would like to thank Hande Türkmen for always being out there for me when I most needed physical and mental support throughout this journey.

TABLE OF CONTENTS

LIST OF TABLES

TABLES

LIST OF FIGURES

FIGURES

LIST OF ABBREVIATIONS

ABBREVIATIONS

AS: Almond Shell

AS-H: Fast Pyrolyzed Almond Shell

AS-L: Slow Pyrolyzed Almond Shell

AS-T: Torrefied Almond Shell

DTF: Drop Tube Furnace

IEA: International Energy Agency

OR: Olive Residue

OR-H: Fast Pyrolyzed Olive Residue

OR-L: Slow Pyrolyzed Olive Residue

OR-T: Torrefied Olive Residue

PM: Particulate Matter

SDS: Sustainable Development Scenario

TL: Tunçbilek Lignite

TL-H: Fast Pyrolyzed Tuncbilek Lignite

TL-L: Slow Pyrolyzed Tuncbilek Lignite

WMR: Wire Mesh Reactor

CHAPTER 1

INTRODUCTION

1.1 World Energy Overview

The energy demand in the World has been escalating due to population growth, industrialization, and technological advancement. Concurrently, the advent of the now termed climate crisis and the considerable slice of carbon emissions attributed to the energy sector have forced governments and private companies to quickly shift towards the development of renewable energy sources such as wind, solar, hydro, geothermal, and biomass. Even though the focus on cleaner energy mostly on the sources of wind and solar, the clean combustion of coal and/or biomass cannot be ignored, as it can often be achieved by retrofitting conventional coal power plants.

In the last two decades, the power generation from bioenergy has increased by 346%, from 132 TWh in 2000 to 589 TWh in 2019. [1] In Sustainable Development Scenario (SDS), the power generation from 2019 to 2030 is expected to increase by 100%, as shown in Figure 1.1.

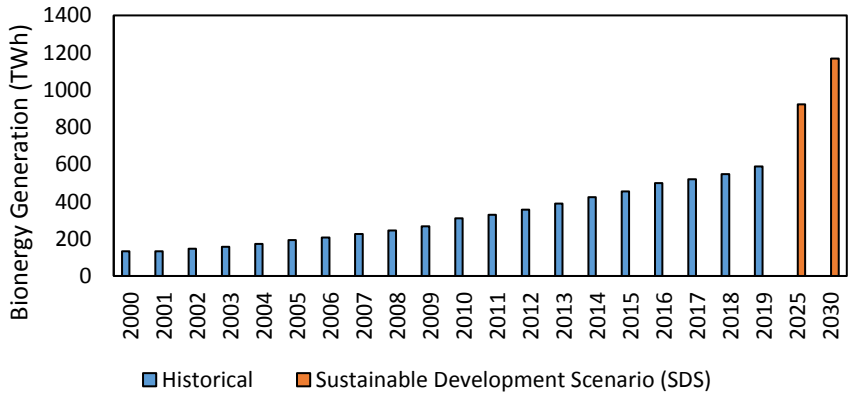

Figure 1.1 Bioenergy generation in the Sustainable Development Scenario, 2000 - 2030 [1]

To achieve the sustainable development on power generation from bioenergy, incentive mechanisms from the part of governments are already in place for (i) the clean utilization of fossil fuels through 1st and 2nd generation combustion technologies; (ii) the usage of renewable energy sources such as biomass in 100 % biomass firing and coal-biomass co-firing power plants; and (iii) the development of mitigation technologies such as carbon capture utilization and storage (CCUS).

In 2015, coal and lignite in Turkey provide a combined 31.6 % of the total energy supply. In contrast, biomass feedstocks represent only 2.6% [2,3] despite Turkey's strong agricultural component that generates large quantities of residues that can be transformed into value-added bioresources. However, in 2018, the energy supply from the bioenergy consisted of wood, biomass, and animal waste increased to 3.3%, as seen in Figure 1.2.

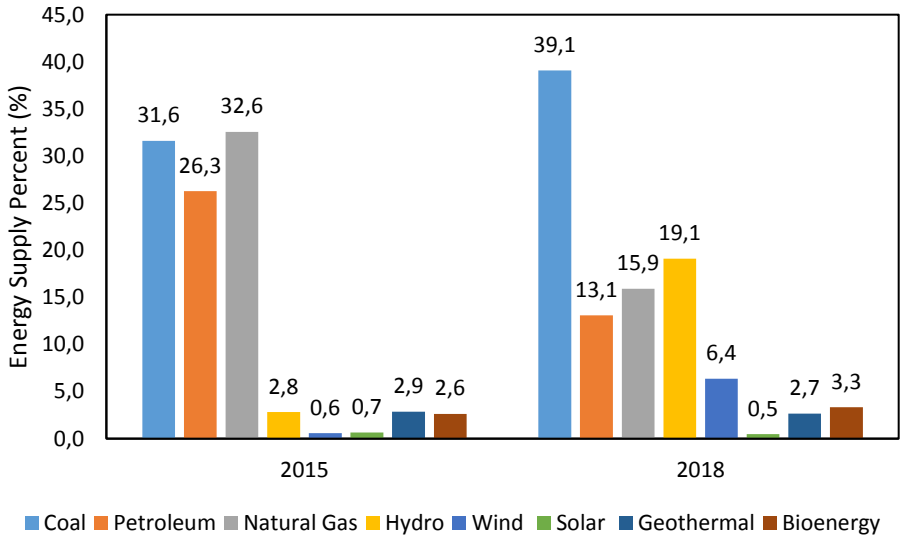

Figure 1.2 Electricity generation of Turkey from different sources [2,3]

Due to the considerable and expected increase in biomass firing for energy supply in recent and upcoming years, co-firing and biomass firing technologies must be highly focused. Co-firing and biomass firing can provide a route for clean, flexible, and low-cost energy generation. However, discrepancies between coal and biomass feedstocks may result in difficulties during transportation, pre-processing, and

burning in existing coal boilers. Agricultural biomass, in particular, presents additional shortcomings such as high moisture content, high heterogeneity among feedstocks, and poor grindability. Despite these difficulties, co-firing is seen as one of the most cost-effective methods of converting biomass to biopower and receives significant attention in the World [4,5].

Co-firing can be advantageous since fossil fuel usage decreases, fuel costs and emissions of NOx and CO2 are reduced, waste is minimized, and soil and water pollution is reduced [6]. However, due to the increased formation of deposits in the boiler and ash use limitations due to chemical components in biomass, attention must be taken. Using biomass in a co-firing application has some advantages and disadvantages.

The advantages of using biomass for co-firing are:

1) Biomass combustion is accepted as carbon-neutral process [4]. CO_2 released to the atmosphere during the biomass combustion is considered to be compensated with the CO_2 removed from the atmosphere with photosynthesis [7].

2) The bottom and fly ash of biomass can be used as a soil additive in the agricultural industry [4] and it would be more cost effective than the disposal of the ash [8,9].

3) By biomass combustion, CH_4 release of landfilled biomass is avoided. Moreover, when co-fired, the NO_x and SO_x emissions are reduced [10–12]. Also, S in coal can be advantageous in preventing sticky deposits by converting KCl to K_2SO_4, which is less harmful [12].

4) The energy required to produce and gather biomass is more than it is produced during the combustion. However, the cost of the energy produced from biomass is still less than the cost of the energy produced from fossil fuels [13,14].

5) Biomass usage increases the employment rate since it encourages the local investment [6].

The disadvantages of using biomass for co-firing are:

1) Biomass storage should be sized for daily supply of biomass to keep the power plant operating since there might be supply shortages [8,9].

2) Besides the storage, the fuel handling units and feeding units for biomass must be larger than the ones designed for fossil fuels [8,15–18].

3) The high percentages of alkali, such as potassium, chlorine and other inorganic elements in ash are the major source of concern [12], which may result in fouling, slagging and agglomeration in the combustion chamber.

Even though there are environmental and techno-economic concerns on biomass, none of these represent an irresolvable obstacle. To solve the risks of biomass; co-firing, pre-processing of the biomass, additives, and alternative materials (such as different alloys) usage for combustion chamber structure can be applied individually or combined [12]. However, due to the disadvantages mentioned previously, the biomass shares in a co-fired power plant using a fluidized bed combustor are announced as being usually limited to 20% of the total fuel used [19].

1.2 Motivation

Around 40% of the total electricity is still generated from coal [20]. Coal is a fossil fuel and emitting high amounts of CO_2 to the atmosphere. Hence, the greenhouse emissions and fossil fuel use must be reduced. To achieve this, the already operating power plants must be converted into 100% biomass-fired or coal – biomass co-fired power plants since the transition from coal-fired power plants to these technologies would require a small number of changes. The biomass and coal single particle combustion behavior must be investigated to gradually replace the currently burned lignites with biomass fuels and transiting coal power plants to biomass and co-fired power plants. This thesis aims to understand the combustion behavior of single-particle coal and biomass fuels. The knowledge would present more information to better view the design problems of the mentioned systems.

1.3 Objective

The main objective of this thesis is to understand the combustion behavior of the studied Turkish biomass and lignite. To achieve this objective, single-particle fuels must be observed closely to understand their ignition modes. Also, characterization of the fuels for their ignition delay times, volatile and char combustion times, and burnout times is required. Moreover, single-particle combustion experiments must be conducted to understand the effect of pre-treatments (torrefaction and pyrolysis) on the ignition modes and combustion times.

CHAPTER 2

LITERATURE REVIEW

This chapter consists of four main sections. In Section 2.1, an overview of biomass and coal combustion is introduced. In Section 2.2, the fundamentals of thermal pre-treatment methods are explained. In Section 2.3, the selected state-of-the-art studies on single-particle combustion are investigated. In Section 2.4, the state-of-the-art studies on wire mesh reactor are examined.

2.1 Coal and Biomass Combustion

Coal is a high amount of carbon and hydrocarbons inclusive, black or brownish-black rock which can combust [21]. It is originated from dead plants and animals which are pressurized underground for millions of years. Since it takes a long time for coal to form, it is classified as a nonrenewable energy source [22]. Dead plants and animal remain were converted to peat, lignite, sub-bituminous coal, bituminous coal, and anthracite with the effect of pressure and heat over millions of years underground.

Lignite has the lowest energy content of all fuels. It is the youngest coal type, resulting in high moisture content and low heating value. Sub-bituminous coals are the second youngest coal types. The formation time of the sub-bituminous coal is around 100 million years. Between 100 to 300 million years, bituminous coals are formed. The carbon content and heating value of the bituminous coals are higher than sub-bituminous coals [22,23]. The oldest coal is anthracite. Due to its high carbon content, it is more dense, harder, and brighter than the other coal types. Due to it is rareness and hardness of processing, other types of coal are primarily preferred

in commercial applications. The carbon contents of the mentioned coal ranks are shown in Table 1.

Table 1 Carbon content of coal ranks [22,24]

Ranking	*Carbon Content (%)*
Peat	< 25
Lignite	25 - 35
Subbituminous	35 - 45
Bituminous	45 - 86
Anthracite	86 - 97

Biomass is renewable organic fuel that is produced from plant and animal wastes. Biomass sources for energy generally include wood and processed wood wastes (i.e., wood pellets, wood chips, sawdust), agricultural crops and their waste (i.e., olive residue, almond shell, hazelnut shell, corn, soybeans, sugar cane, etc.), municipal solid waste (i.e., paper, cotton, wool, food wastes, etc.), animal manure, and human sewage.

The energy in biomass can be converted as biological conversion or thermochemical conversion. In biological conversion technologies, biogas that mainly consisted of CH_4 and CO_2, is produced from biomass. The conversion process is done through four steps: starting from hydrolysis, continuing with acidogenesis then acetogenesis, and finishing with methanogenesis [25]. These processes are referred as anaerobic digestion and it is a widely used technology especially for producing biogas out of municipal waste. Biogas can be used in different energy generation processes [26].

Thermochemical conversion is consisted of two main categories, which are gasification and combustion. In gasification process, the biomass undergoes incomplete combustion with gasifying agents (i.e., air, oxygen, and steam) so that the product gas after the reaction can become potentially combustible. For gasification, the biomass undergoes the processes in the order of drying, pyrolysis,

oxidation, and reduction. The product after the gasification process is called syngas and it can be used in gas turbines, fuel cells and reciprocating engines [27].

The second thermochemical conversion technology is the reaction of combustion, which occurs when fuel is combined with an oxidizer and undergoes a self-sustained exothermic chemical reaction [26]. For the combustion of hydrocarbon fuels, the oxidizer is oxygen. The combustion reaction also has an activation energy limitation as all reactions. The reaction is triggered as the activation energy limit is surpassed with sufficient heat supply, and the fuel-oxidizer mixture is within the flammability limits [21]. Due to that, the products of the combustion reaction depend on the fuel and on the active sites, such as the carbon sites that oxygen can react with. The reactions below are the combustion reaction examples for different fuel types:

$$4\ C_aH_b\,(g) + (4a + b)\ O_2\,(g) \rightarrow (2b)\ H_2O\ (g) + (4a)\ CO_2\,(g) \quad (1)$$

$$H_2\,(g) + 1/2\ O_2\,(g) \rightarrow H_2O\ (g) \quad (2)$$

$$C\ (s) + O_2\,(g) \rightarrow CO_2\,(g) \quad (3)$$

where equation (1) represents the combustion of hydrocarbons, equation (2) represents hydrogen combustion, and equation (3) represents carbon combustion. The combustion reactions are incomplete when there is insufficient time or oxygen. Along with the products mentioned above, CO also occurs in incomplete hydrocarbon and carbon combustion products.

Depending on the physical state of the fuel–oxidizer, the combustion reaction can be classified as homogeneous and heterogeneous reactions [21]. The combustion reactions that are occurring in a single-phase are called homogeneous reactions. Methane combustion with oxygen can be an example of a homogeneous combustion reaction [28]. On the other hand, the reactions in two or more phases are called heterogeneous combustion.

Solid fuels' combustion is a complex reaction in which diffusional mass transfer and surface reaction kinetics are coupled. Solid fuel combustion can be classified into four

stages: drying, devolatilization, volatile combustion, and char combustion. The solid combustion process is visually summarized in Figure 2.1 [21]. It must be noted that, for some fuels, the steps of solid fuel combustion would not be seperated easily. To illustrate, for some coals, devolatilization and char combustion tend to happen simultaneously [29–31]. After the combustion process of solid fuels, ash is left as residual (inorganics in the fuel).

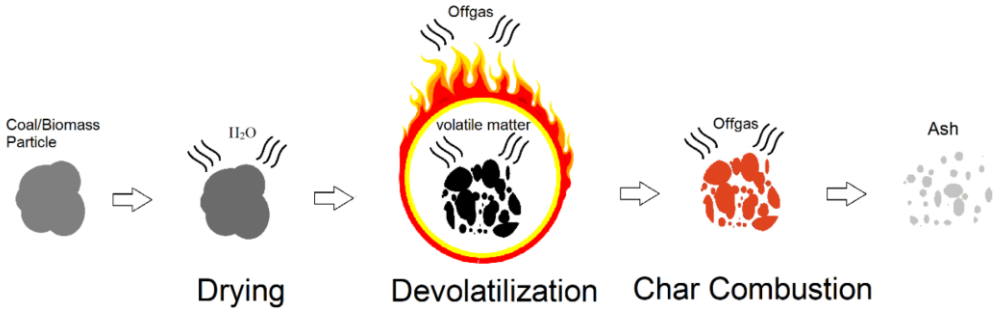

Figure 2.1 Steps of solid fuel combustion: drying, devolatilization, char oxidation [21]

For solid fuels, first, the drying stage takes place. In this stage, the gases stored in the pores of the fuel's structure are desorbed around the temperature of 100 ºC. Some of these gases are water steam, nitrogen, methane, and carbon dioxide [32]. The Devolatilization stage takes place above 400 ºC. The temperature for devolatilization to start is depending on the composition of the solid fuel. The Devolatilization stage has three specific physical and chemical processes [21]. These processes are: 1) pyrolysis, which is the decomposition of the fuel, 2) transportation of the volatile matter through the pores of the fuel, and 3) secondary reactions that may occur by providing sufficient volatile residence time and allowing the volatile matter decomposition to other gases [33]. After devolatilization, only char is left. At the end of the char combustion, the particle is only left with the ash.

2.2 Thermal Pre-Treatment Studies

Co-firing and biomass firing can provide a route for clean, flexible, and low-cost energy generation. However, discrepancies between coal and biomass feedstocks may result in difficulties during transportation, pre-processing, and burning in existing coal boilers. Agricultural biomass, in particular, presents additional shortcomings such as high moisture content, high heterogeneity among feedstocks, and poor grindability. In recent years, thermochemical pre-treatments such as torrefaction, slow pyrolysis, and hydrothermal carbonization have emerged as suitable candidates for obtaining a processed biomass fuel (biochar) that more closely resembles coal in both its chemical and physical properties.

2.2.1 Pyrolysis

Pyrolysis is the first step in coal and biomass combustion and a widely applied thermochemical process for the production of value-added chemicals, including the production of biochar. The biochar yield can be maximized if pyrolysis occurs at medium temperatures (300-700 ºC) and over hours or days since polymerization reactions are allowed to occur. Slow pyrolysis has the added advantage of allowing disparate-sized feedstocks to reach a similar value of solid yield, even with particle sizes ranging from 5 to 50 mm [34]. The biochar obtained from slow pyrolysis presents high carbon (53-96 %) and high heating values ranging from 20 to 36 MJ/kg. The products and their used areas are shown in Figure 2.2.

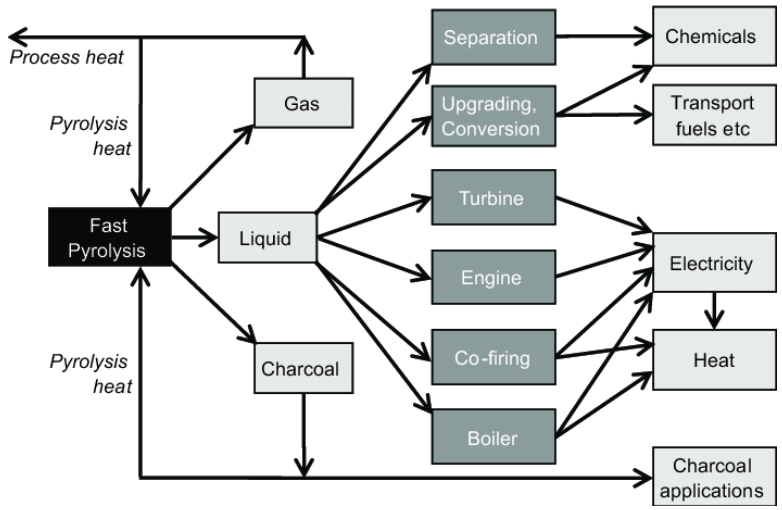

Figure 2.2 Products from thermal biomass conversion. [35]

The physical and chemical properties of coal and the conditions of the combustion process can affect the pyrolysis behavior [36–38]. Volatile release from the particle can often cause swelling due to internal pressure increase, and due to the high porosity, it may result in fragmentation. Moreover, the environmental conditions also affect the amount of volatiles released. The volatile release increases with a high heating rate [39]. If there is oxygen in the environment, the released volatile matter can oxidize simultaneously under the flammability limits.

The yield, structure, shape, and surface area of the produced chars are affected by the heating rate during pyrolysis. Even though thermogravimetric analyzers (TGA) [40–42] have shown a considerable influence of heating rate change (range of 1 to 10 ^{o}C/s) on pyrolysis behavior, new studies utilizing wire mesh reactors [43–47] have allowed for greater rates (10^{3} ^{o}C/s) and investigation of fast pyrolysis [48]. During wire mesh reactor experiments, the heating rate of the particle is expected to be similar to the wire mesh itself due to the close contact between the mesh and the sample and low amount of the latter. The influence of operational parameters on biomass pyrolysis has been thoroughly reviewed in recent publications [34,49].

During the process of pyrolysis of coal and biomass, an unstable intermediate phase – metaplast is formed [50], which controls the char particle's subsequent softening. Cross-linking usually occurs before bridge-breaking at low heating rates, reducing char plasticization [51]. Since bridge-breaking happens before cross-linking [51], plasticization is enhanced at high heating rates, leading to increased fluidity, significant melting, and char swelling [48]. Trubetskaya et al. [51] and Panahi et al. [52] observed that biomass chars exhibited significant deformation, as well as the production of macro-pores and considerable melting at high heating rates. Also, Le Manquais et al. [47] reported significant swelling associated with the plasticization of coal chars produced by high heating rate pyrolysis.

2.2.2 Torrefaction

Torrefaction, also termed mild pyrolysis, consists of heating raw biomass typically at 200–300 °C under an inert atmosphere, from there eliminating moisture and light hydrocarbons. Since the required temperatures are relatively low, these released volatile hydrocarbons are often used as a heat source to self-sustain the process. The resulting fuel has higher calorific content 21-33 MJ/kg [53], longer shelf-life, and increased grindability [54–56].

Van der Stelt et al. [55] stated that the torrefaction process is based on the removal of oxygen from biomass, aiming to increase the energy density of the fuels by decomposition of the reactive hemicellulose fraction. Colin et al. [56] investigated the optimization of the torrefaction process. They stated that the moisture uptakes for mass losses above an optimum (a mass loss between 1.7% and 7.8%) remain stable at values twice lower than that of raw biomass. Bridgeman et al. [54] observed that after the torrefaction process, the volatile composition of the biomass fuels are reduced and these fuels became more thermally stable. Also, these fuels produced greater heats of reaction during the combustion process.

Besides the combustion behavior, torrefaction process is also influencing the PM formation of biomass fuels. Biomass combustion often produces higher quantities of sub micrometer PM [48,57–60]. Shao et al. [57] observed that the PM values increased when corn stalk was torrefied comparing to raw feedstock, and due to the decrease of Cl and S after torrefaction and presence of K2SO4, they attributed it to the increase in PM0.1-1. On the other hand, Han et al. [61] concluded that due to the vaporized K transformation into the coarse particles, lower levels of PM1 is observed in the rice husk torrefaction. Wang et al. [62] related the yields of PM0.3 to the Cl presence in the thermal pre-treated biomass during the analysis of the effect of hydrothermal carbonization, torrefaction pre-treatment, and slow pyrolysis of straw.

2.3 Single Particle Studies

In recent years, with the development of affordable high-speed optical methods, single-particle devices such as optical drop tube reactors; flat flame or Hencken burners; and wire mesh reactors gained popularity and are now widely used to analyze the ignition and combustion of biomass and coal fuels under high heating rate and high temperature [30,63–70]. Researchers use single-particle experimental setups and focus on (i) analyzing the differences between biomass and coal combustion [64], (ii) the determination of milling requirements for biomass fuels [67–69], (iii) the analysis of the influence of torrefaction during biomass combustion [69,71–74], (iv) the identification of the typical combustion phenomena such as volatile flame size and char fragmentation [52,63,75–77], and finally (v) on the quantitative determination of single-particle combustion times and temperatures [66,78–83].

Mason et al. [68] used a Méker type natural gas burner and combusted single particle woody biomass fuels to evaluate the empirical expressions for the relationship between particle mass and ignition delay, volatile flame duration and char burn duration. Mock et al. [69] combusted a torrefied and a raw biomass fuel along with a lignite by using a laboratory-scale entrained single particle reactor which controlled

its gas temperature, flow velocity, and oxygen concentration by the postcombustion gas, guard heater, and water-cooled injector. They observed that flame volatility is not only mainly related to the particle's volatile matter content, but also attributed to soot formation. Biomass has a relatively more volatile content than coal and yields a less sooty flame, but a stable flame is detected for torrefied biomass fuel even at the smallest pulverized particles.

Magalhaes et al. [75] used a McKenna flat flame burner to investigate the combustion behavior of single particle biomass and lignite fuels. They observed that all the solid fuels generally ignited in the gas-phase. Also, they observed that the ignition delay times tended to decrease when the atmosphere temperature increased. However, they added that on ignition delay times, the impact of the oxygen concentration in the atmosphere was insignificant.

Lei et al. [79] used a drop tube furnace for single particle combustion experiments and observed that the ignition delay time was increased and the combustion temperatures decreased when N_2 was replaced by CO_2. Also, Magalhaes et al. [30] investigated the effect of torrefaction of biomass on single-particle combustion to select an alternative fuel for lignites by using a Drop Tube Furnace (DTF). They observed that the burnout times of biomass fuels which are raw and torrefied were similar to those of Tunçbilek lignite but more prolonged than Soma lignite. The experimental setup used by Magalhaes et al. [30] is shown in Figure 2.3.

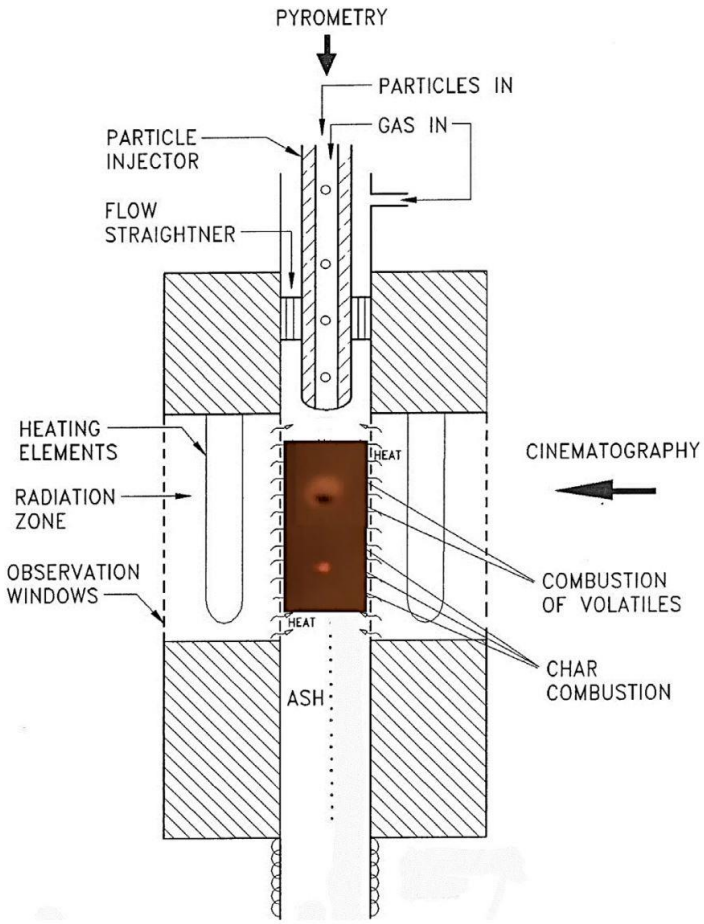

Figure 2.3 Drop tube furnace schematic used by Magalhaes et al. [30]

Also, the same behavior of torrefied fuels are observed by Panahi et al. [84]. They observed that differently sized torrefied biomass (212 – 300 μm) and coal (75 – 90 μm) fuels had similar burnout times. He concluded that using larger sized torrefied fuels would reduce the grinding costs of the operating power plants. Moreover, Vorobiev et al. [73] observed that even the shape of the torrefied fuel was different; in other words, the fuels with high aspect ratio, became rounded after the combustion process. They also added that the torrefaction process reduced the char burnout times. Panahi et al. [74] observed that in torrefied fuels, the oxygen fraction in oxygen – carbondioxide atmosphere is mainly influencing the ignition delay time of the fuels and their combustion behaviors, such as the combustion temperature.

To better understand the single particle combustion behavior of the biomass and lignite fuels, studies in the literature use wire mesh reactors due to devices' easiness of operation, flexibility, and optical access. Wire mesh reactors can have both high and slow heating rates, and the configuration can be changed easily.

Flower et al. [70] used a wire mesh single particle experiment setup to conduct single particle biomass combustion for particles ranging from 5 to 30 mg to determine the effect of particle size on the combustion and observed that the dependency on the aspect ratio of the samples is relatively low.

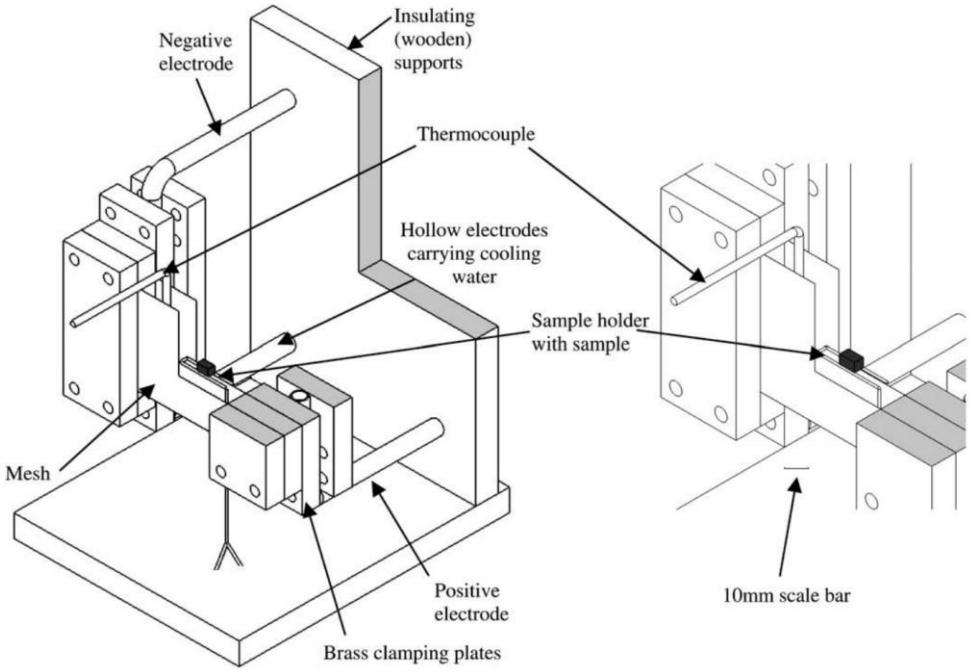

Figure 2.4 Cut away diagram of wire mesh apparatus used by Flower et al. [70]

Riaza et al. [64] performed single-particle experiments in a wire mesh reactor to observe the relationship between particle mass and burnout time. They observed that the predominant parameter that affects the burnout time was the particle mass. Moreover, in another study by Riaza et al. [67], they performed single-particle experiments in a wire mesh reactor in order to understand the shape change of the biomass particles and observed that the biomass particles became round after the combustion.

Besides the single-particle experiments, wire mesh reactors can also be used for pyrolysis experiments. Creating an inert atmosphere can be easier than other reactors since the volume of the reactor chambers is relatively small. Magalhães et al. [44] and Trubetskaya et al. [51] used wire mesh reactor with different temperature zones and heating rates to develop a model to predict the yields and composition of chars.

CHAPTER 3

EXPERIMENTAL METHODOLOGY

In this Chapter, the characterization of fuels in this study are described. Moreover, the reactors and experimental methodology used in this study are outlined.

3.1 Fuel Selection and Preparation

In this study, three endogenous resources of Turkey were selected: olive residue (OR), almond shell (AS), and Tunçbilek lignite (TL), which is lignite coal from Tunçbilek power plant. Olive residue is an agricultural waste from olive/olive oil production and was supplied by Forazeytin, located at Havran, Balıkesir region. The company Forazeytin pre-dries the olive residue below 10 wt% moisture and delivers them grounded to 5 mm and below. Almond shell is an agricultural waste from almond harvesting in the Mersin region. The cooperative Bademder delivers the almond shell chunks without any pre-process. Tunçbilek lignite was mined in the region of Tunçbilek – Tavşanlı, Kütahya and was supplied by the Turkish Coal Enterprises (TKI). The origin provinces of the selected fuels are shown in Figure 3.1.

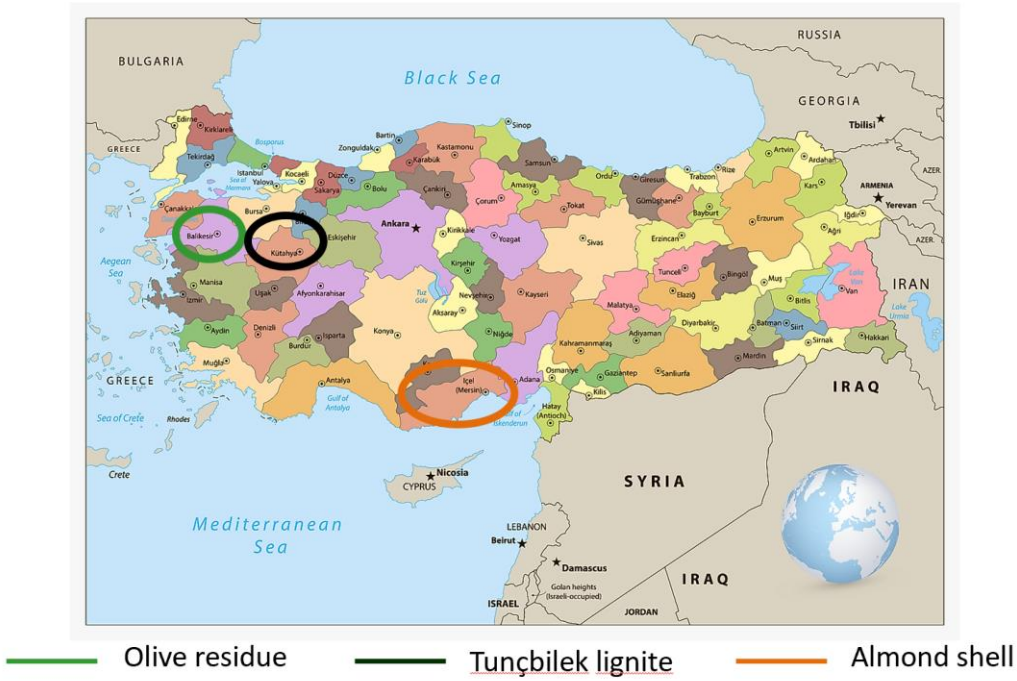

Figure 3.1 Origin of selected agricultural residue and coal in Turkey

The annual tonnages of Tunçbilek lignite is 7 Mt [85]. The supplier (TKI) washed the lignite coal before the transportation to remove most mineral matter excluded. A float and sink test, which is commonly applied to handle high-ash coals such as Turkish lignites, was performed for the washing process [86]. Photographs of olive residue, almond shell, and Tunçbilek lignite (as received) are shown in Figure 3.2.

Figure 3.2 (a) Olive Residue, (b) Almond Shell, and (c) Tunçbilek lignite. A size bar is included at the bottom right [48].

All samples were initially ground and sieved to a particle size range of 1-3 mm. This size range emulates the upper range in biomass-fired power plants. The ground and sieved fuels were used in raw, torrefied, and pyrolyzed forms. All samples were fully characterized for their ultimate and proximate analyses based on standard procedures. The proximate analyses for the fuels were obtained by using a Perkin Elmer 4000 thermogravimetric analyzer by applying the procedure described by Mayoral et al. [87]. The ultimate analyses for the fuels were undertaken according to the standard D5373-16 and carried out by the METU Central Lab. The heating values were also calculated based on adequate correlations [88,89]. The chemical composition and heating values are presented in Table 2. The ultimate analysis of the Tunçbilek lignite differs from other studies on the same lignite [90,91]. The coal seam may be different, and the batch we receive is washed before removing the external inorganics to enrich the fuel. The washing process was performed by a float and sink test [92].

Table 2 Ultimate and proximate analysis of the studied fuels

Parameter	*Olive Residue (OR)*	*Almond Shell (AS)*	*Tuncbilek Lignite (TL)*	*Olive residue torrefied (OR-T)*	*Almond shell torrefied (AS-T)*	*Olive residue - Fast Pyrolyzed (OR-H)*	*Almond Shell - Fast Pyrolyzed (AS-H)*	*Tuncbilek Lignite - Fast Pyrolyzed (TL-H)*	*Olive Residue - Slow Pyrolyzed (OR-L)*	*Almond Shell - Slow Pyrolyzed (AS-L)*	*Tuncbilek Lignite - Slow Pyrolyzed (TL-L)*
Proximate Analysis (wt %, dry basis)											
Volatiles	76.4	79.8	32	67.2	68.7	19.9	21.7	14	10	12.7	7.5
Fixed Carbon[a]	18.5	19.2	53.6	28.7	26.4	74.7	73.2	47.8	80	84.8	63.9
Ash	5.1	1	14.4	4.1	4.9	5.4	5.1	38.2	10	2.5	28.6
Ultimate Analysis (wt %, dry basis)											
C	46.6	45.4	61.8	56.6	56.5	72.9	83.2	82.5	84	91.5	71.7
H	6.4	6.3	5.6	5.8	6	0.4	0.7	1.4	0	0	0
N	0.6	0.4	2.7	0.3	0.2	0.7	0	2.8	0.9	0.6	2.2
S	0	0	1.5	0	0	0	0	0.5	0	0	0.5
O[a]	46.4	47.9	28.5	37.3	37.3	26	16.1	12.8	15.1	7.9	25.6
HHV (MJ/kg)	19	18.4	27.8	22.8	22.9	23.2	28.1	20.2	27.7	31.1	24

[a] by difference

3.2 Experimental Setup

3.2.1 Thermogravimetric Analyzer

A thermogravimetric analyzer (TGA) is an extensively used reactor to study material behavior under different thermal conditions. A TGA includes the following tools to conduct a proper experiment: 1) a furnace in which the material sample is placed, 2) a thermocouple to monitor and record the temperature during the experiment, 3) a microscale to monitor and record the weight, 4) valves and mass flow controllers to control the inlet of the gas, and 5) a PC [48]. In this study, a PerkinElmer STA 4000 Thermogravimetric Analyzer is used. The used reactor is located at the Composite Material Characterisation Laboratory, Center for Wind Energy Research, Middle East Technical University. During the experiments, weight loss profiles of the samples as a function of temperature and/or time were obtained for proximate analysis. A Fourier-transform infrared (FTIR) spectrometer was coupled with the PerkinElmer STA 4000 reactor to gather online gas composition data, as represented in Figure 3.3.

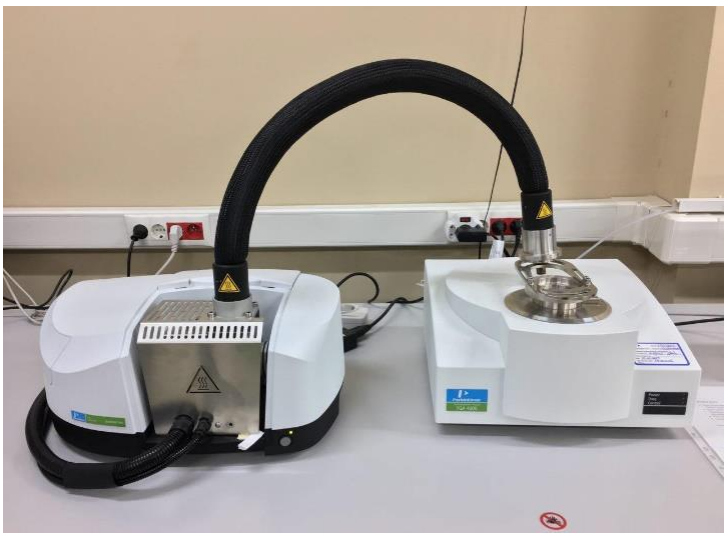

Figure 3.3 TGA coupled with an FTIR spectrometer at the Composite Material Characterisation Laboratory at Center for Wind Energy Research, Middle East Technical University [48].

3.2.2 Horizontal Furnace

For the torrefaction and slow pyrolysis experiments, a Protherm PFT series tubular furnace is used. The furnace can reach up to 1400^{o}C, the residence time can be preset and the atmosphere can be changed [93]. The photograph of the tubular furnace used is shown in Figure 3.4 and the sketch of the furnace is shown in Figure 3.5.

Figure 3.4 Horizontal furnace used for torrefaction and slow pyrolsyis experiments

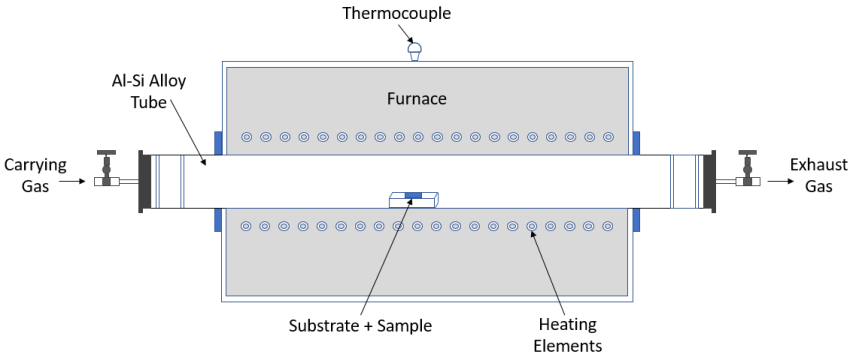

Figure 3.5 Sketch of horizontal furnace used for torrefaction and slow pyrolysis experiments

3.2.2.1 Slow Pyrolysis

Slow pyrolysis experiments are done using the horizontal furnace for all fuels (OR, AS, and TL) at 10 ºC/min, and at a plateau temperature of 1000 ºC (in line with the temperature chosen during fast pyrolysis trials). Slow pyrolysis pre-treatment applied under 100 % N_2. First, the ground and sieved individual particles were weighed (as shown in Figure 3.6) and placed in a crucible inside the furnace (as shown in Figure 3.7) to conduct the slow pyrolysis experiment.

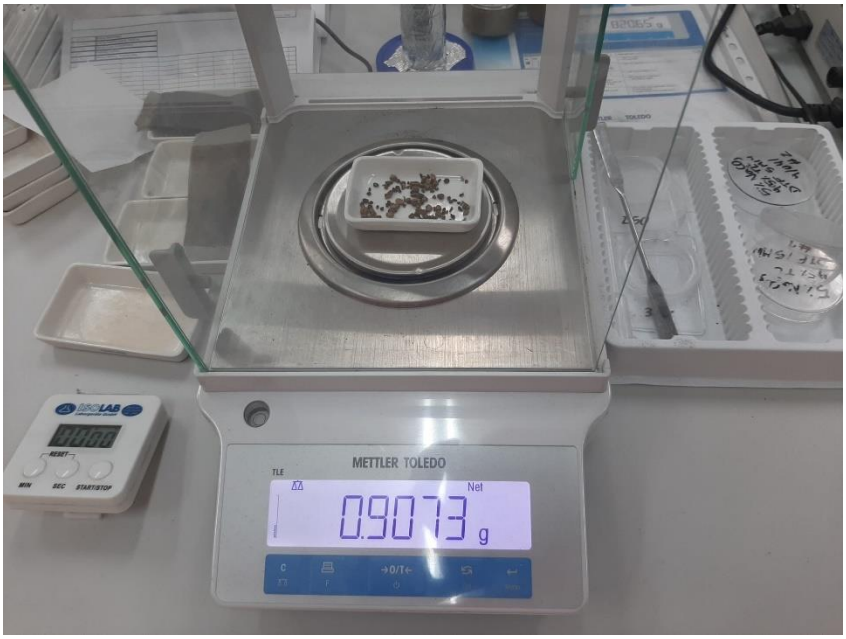

Figure 3.6 Olive residue particles weighted for slow pyrolysis experiment

Figure 3.7 Olive residue particles put into the horizontal furnace for slow pyrolysis experiment

Then, both ends of the furnace were fitted, and N_2 at a rate of 10 slpm was allowed to flow for approximately 10 min to ensure sufficient volume changes that guaranteed no oxygen present. Upon the end of the program, the samples were cooled in the furnace under nitrogen flow, and when the furnace temperature reached 150 ºC, the samples were removed and stored in glass vials until further analysis.

3.2.2.2 Torrefaction

Torrefaction and slow pyrolysis were conducted in the same experimental procedure. Torrefaction was performed for both OR and AS at a heating rate of 10 ºC/min and plateau temperature of 275 ºC inside the inert atmosphere of N_2. Upon reaching the plateau, the temperature was held for 60 minutes to ensure complete torrefaction. When the furnace temperature reached 150 ºC, the samples were removed and stored in glass vials until further analysis, as shown in Figure 3.8.

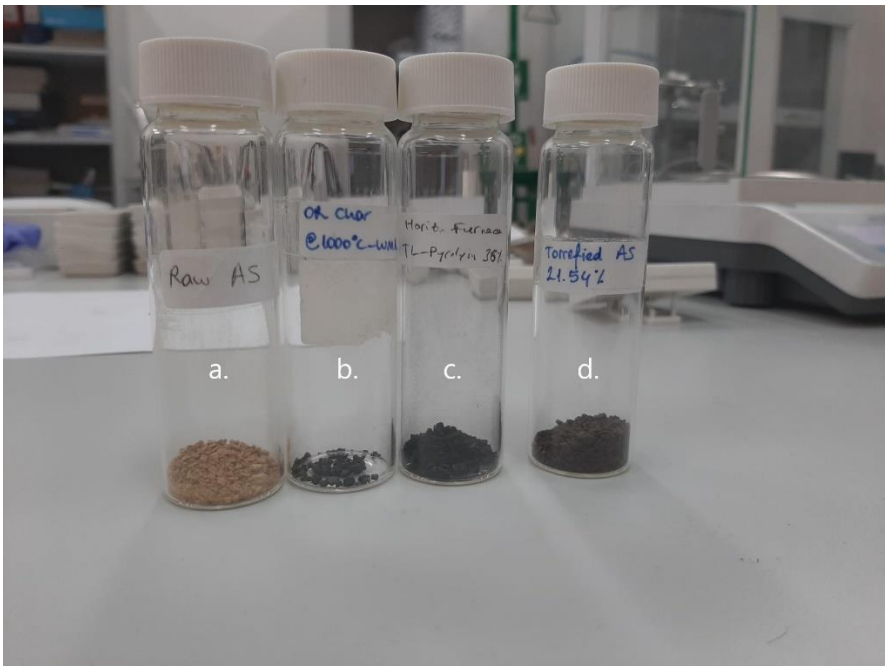

Figure 3.8 Pre-treated and raw fuels ready for single particle combustion experiments (a. Raw almond Shell, b: fast pyrolyzed olive residue, c: slow pyrolyzed Tunçbilek lignite, and d: torrefied almond shell)

3.2.3 Wire Mesh Reactor

3.2.3.1 Fast Pyrolysis

A wire mesh reactor (WMR) in a horizontal configuration was used to fast pyrolyze all samples under high temperature and high heating rate conditions [48]. The WMR used herein comprised an SS-316 wire mesh, conductive electrodes, a welding machine as a power source, a thermocouple, a glass chamber, and a pressure gauge, as represented in Fig. 2. Further details of the WMR used in this work can be found elsewhere [94]. The pyrolysis conditions, defined based on previous knowledge of the current temperature curves, were a heating rate of 900 ºC/s and a plateau temperature of 1000 ºC held for 10 s. The sketch and photograph of the WMR is shown in Figure 3.9 and Figure 3.10, respectively.

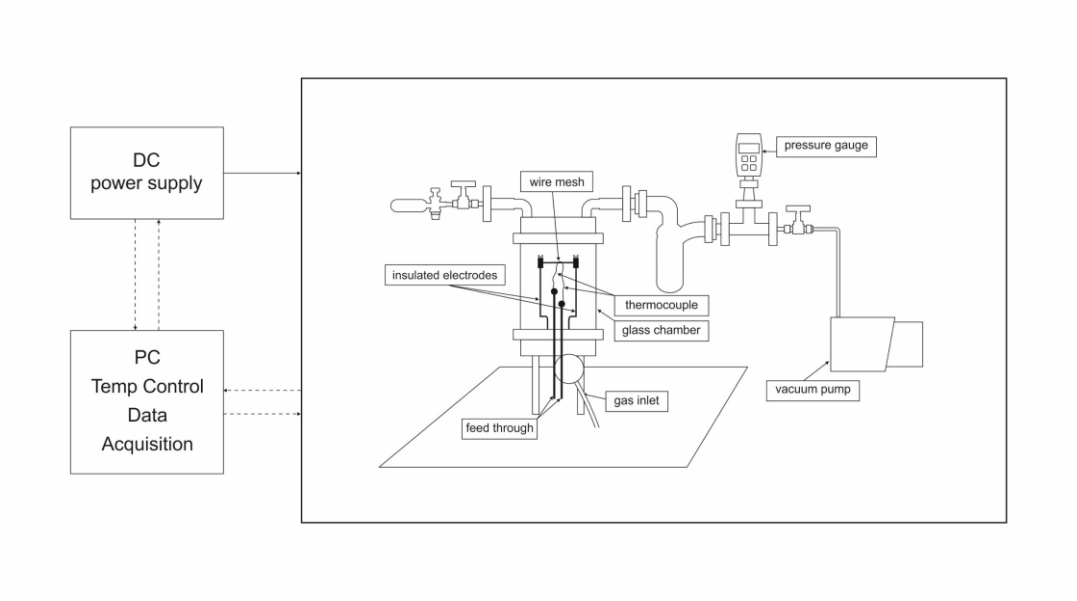

Figure 3.9 Sketch of the horizontal wire mesh reactor (WMR) [94]

Figure 3.10 Photograph of the horizontal wire mesh reactor (WMR) [94]

The methodology during fast pyrolysis in the WMR was as follows: (1) the single particles were weighed and spread between the meshes; (2) the glass chamber was assembled with the reactor and vacuumed to 3 mbar pressure; (3) N_2 was introduced into the chamber until the pressure reaches to atmospheric pressure; (4) the heating rate of the setup and temperature were selected based on the knowledge of the voltage and current values of the used welding machine; (5) the reaction was triggered using software LabVIEW, and the meshes was heated to the predefined temperature and hold at that temperature with a specified time; (6) after completion, the mesh was left to cool down under inert atmosphere it reaches to room temperature; (7) after reaching to the room temperature, the mesh and the particles were weighed to obtain the values of the char yields, and the chars were collected for further analysis.

3.2.3.2 Single Particle Combustion

The vertical WMR configuration in this study was used for the single-particle combustion trials. The constituent elements of the WMR were the same as in the horizontal configuration described in the previous subsection. The only difference is the position of the wire meshes and the placing of a single particle holder. The vertical WMR consisted of two wire meshes positioned vertically relative to the ground with a gap between them to accommodate the particle holder. The single-particle and the wire meshes were not in contact, and the particle was heated (mostly) by radiative heat transfer. A Phantom Miro C110 high-speed camera, which is shown in Figure 3.11, with 12-bit 1.3 MPx CMOS Sensor was coupled to the WMR to observe and log the combustion events. The camera sensor consists of a CMOS sensor with pixel size 5.6 µm and 1280 x 1024 px resolution. The camera was equipped with a Kowa LM12JCM lens. The camera settings used were a constant exposure time of 1/15000 s and a frame rate of 100 frames per second, which yielded 256 x 256 px resolution. The sketch and photograph of the experimental setup is shown in Figure 3.12 and Figure 3.13, respectively.

Figure 3.11 Phantom Miro C110 High Speed Camera

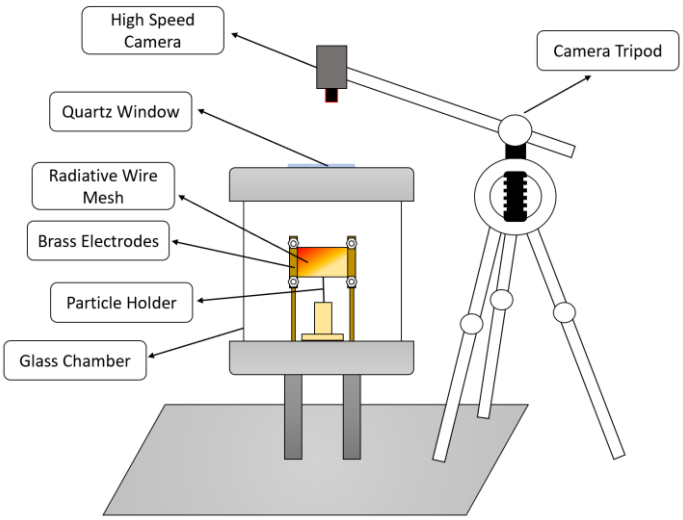

Figure 3.12 Schematic of the vertical wire mesh reactor used for single-particle combustion trials.

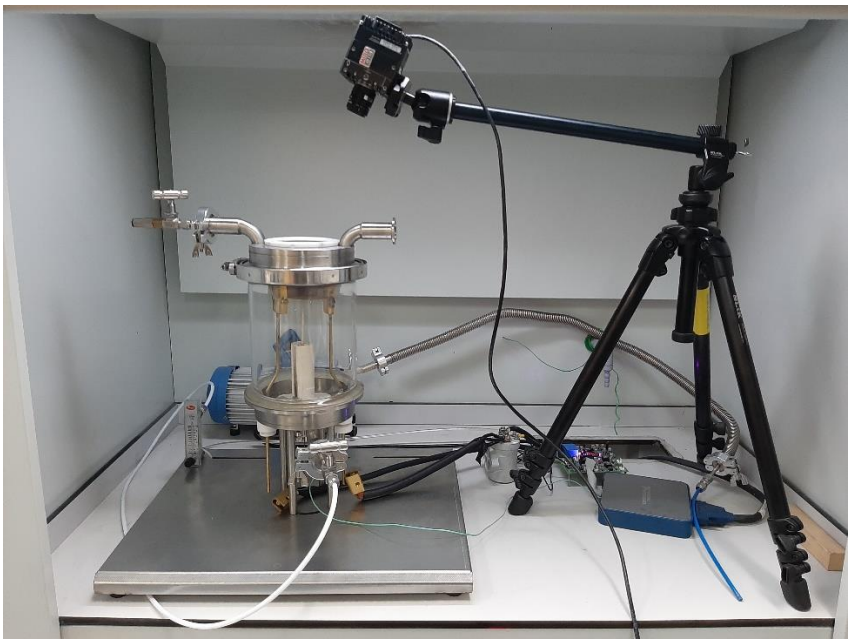

Figure 3.13 Photograph of the vertical wire mesh reactor (WMR) used in single particle experiments

To conduct the single-particle combustion experiments, the following procedure was used: (1) the fuel particle was weighted, and their dimensions; (2) the particle under analysis was placed on the probe, and the chamber was closed; (3) the camera was set with the predefined settings and the exposure time was defined based on a priori knowledge of the typical combustion of each particle; (4) the heating rate of the setup and temperature were selected based on the knowledge of the voltage and current values of the used welding machine; (5) the camera started to record, and the trigger was set to account for the reaction time; (6) the heat source triggered using a LabVIEW interface, and kept on at the specified plateau temperature until burnout was observed; (7) upon completion of the experiment, the glass chamber was removed, and the remaining ash was cleaned from the probe. The combustion conditions chosen were a heating rate of 900 ºC/s with a plateau temperature of 1000 ºC held until the particle reached burnout.

a) b)

Figure 3.14 Olive residue particle dimensions measured to calculate aspect ratio: a) longest diameter, b) shortest diameter

Figure 3.15 Olive residue particle weighted before single particle experiment

Following the recording of the high-speed videos, the saved video frames were pre-processed using MATLAB. The luminosity vs. time curves were used to calculate the combustion times.

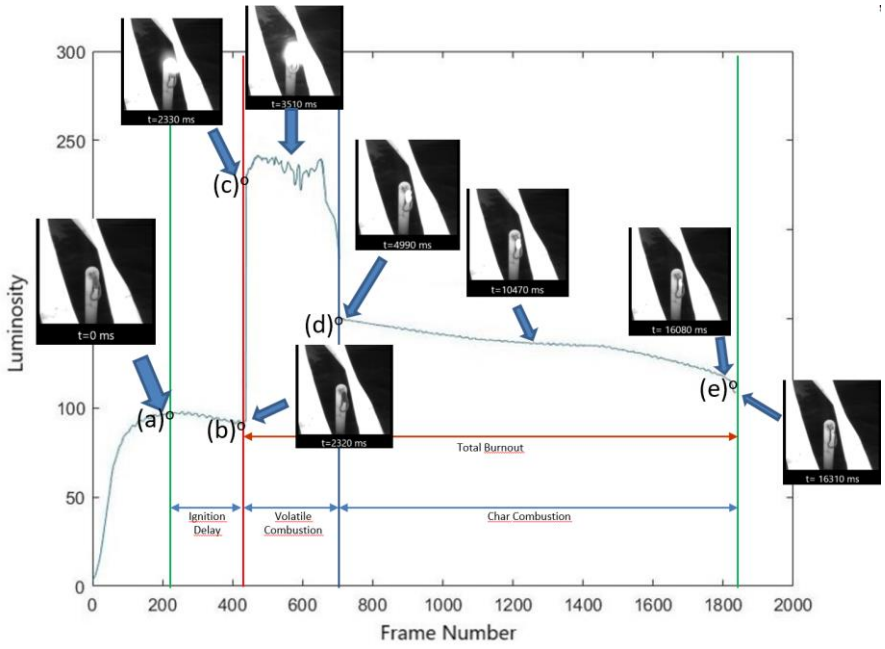

Figure 3.16 Luminosity vs. Frame Number to determine the times in a 100 fps experiment

In Figure 3.16, the graphic that is produced from MATLAB in order to measure the combustion times is shown. It must be stated that the luminosity on each run may be changed due to environmental lighting. In this method, the main objective is to find the luminosity changing points, not the luminosity value itself. The ignition delay time is defined from the instant when luminosity from the particle is stable to the instant (Figure 3.16-a) when the gradient of the luminosity of the particle reaches a maximum (Figure 3.16-b). This maximum gradient point is also used to define the start of the volatile combustion. Until the luminosity gradient goes from negative to zero (Figure 3.16-c), the particle underwent volatile combustion. From the moment of gradient zero (Figure 3.16-d), the particle is defined to have char combustion. The char combustion is defined as the end when a sharp decrease (Figure 3.16-e) in the luminosity demarking burnout occurs. The burnout time is the sum of volatile combustion time and char combustion time for all fuels except chars. For the latter, the char combustion time is equal to the burnout time.

Even though the times are determined using this method, there are measurement uncertainties during each run. Firstly, the scale has a resolution of 0.1 mg during the weighing of the particles. In other words, the reading from the scale is rounded within +/- 0.05 mg. Secondly, in the pre-treatment methods, for slow pyrolysis and torrefaction, the horizontal furnace has a resolution of $1^{o}C$ when it reaches the determined bed temperature. In fast pyrolysis and single-particle experiments, even though the thermocouple used in the wire mesh reactor (WMR) has a resolution of $0.01^{o}C$, the temperature reading has an error of +/- 20 ^{o}C due to the magnetic noise, which is caused by the welding machine used as the power source. To illustrate, the determined bed temperature for WMR experiments is $1000^{o}C$, as explained in Section 3.2.3.1 and Section 3.2.3.2. However, the thermocouple reading is fluctuating between $980^{o}C$ and $1020^{o}C$. Lastly, the camera has a resolution of 0.01s since the experiments are recorded at 100 frames per second. Besides the mentioned errors and uncertainties, there are immeasurable uncertainties during the experiments. Even though each particle underwent pre-treatment or drying, there might be different amounts of moisture inside the particles since each experiment

approximately takes 5 minutes. Starting from the first experiment to the last experiment for each fuel set, the last fuel particle may have increased the amount of moisture. Moreover, the fuel particles are heterogeneous. This heterogeneity (such as hot spots and different structures) results in different combustion times. Due to mentioned errors and uncertainties, the combustion times of the same mass particles may come out differently. For instance, due to the fluctuating bed temperature, the ignition delay time and combustion time of the same mass particles would be different. Also, this difference may occur due to their heterogeneous particle structure or having different particle masses even though the scale shows that they have the same mass. As a result, even the time results are expected to be accurate (around the trend line), they may not be as precise as expected (scattered results may appear). In order to enhance precision and prevent presenting over-scattered results, three experiments are done for each mass interval (1 mg mass interval) for accurate mass-combustion time relation and repeatability.

CHAPTER 4

RESULTS AND DISCUSSION

In this Chapter, the results of the single-particle combustion experiments are analyzed and discussed. In Section 4.1, the ignition and combustion modes of the particles are presented with video cinematography. Then, in Section 4.2, the ignition delay time of each particle is shown. In Section 4.3, the particles' volatile and char combustion times are discussed with the effect of the fuel type and the effect of the thermal pre-treatment methods. Lastly, in Section 4.4, the total burnout times of the fuel particles are presented. Besides the fuel type and thermal pre-treatment effects, the correlation between the aspect ratio of the fuels and the burnout times are discussed.

4.1 Ignition and Combustion Modes

All raw and torrefied fuels were ignited in the gas phase. Following ignition, two-phase combustion (i.e., volatile combustion, followed by the char combustion with no or negligible overlap of the two phases) was observed for all raw fuels, namely olive residue, almond Shell, and Tunçbilek lignite or OR, AS and TL, respectively. Selected high-speed cinematography frames are represented in Figure 4.1 for the raw and torrefied samples. Firstly, the volatiles evolved and burned, and upon extinction of the volatile flame, char oxidation ensued. The torrefied biomass fuels exhibited the same qualitative behavior as the raw fuels. This was also observed in previous works using different single-particle devices [64,65,67,72,75,82], including wire mesh reactor with similarly sized particles [65,67,68]. Even though the combustion mode was the same for all raw fuels, biomass and lignite particles displayed disparate traits during volatile combustion. OR and AS particles showed spherical non-sooty flames surrounding the particle (see Figure 4.1 a.3, a.4, b.3, and b.4), while for TL

the ejection of volatiles and formation of soot trails was observed. OR and AS present higher porosity than TL, thus volatiles can be released easily [95]. On the other hand, the lower porosity of the lignite particle did not allow the prompt release of volatiles [96], and the swelling of TL before ignition due to volatile accumulation and pressure built-up was observed. This swelling before ignition is typical of high volatile bituminous coals [64]. Therefore, TL showed the behavior of bituminous coal with both swelling prior to volatile release and soot trail formation during volatile combustion [30,97].

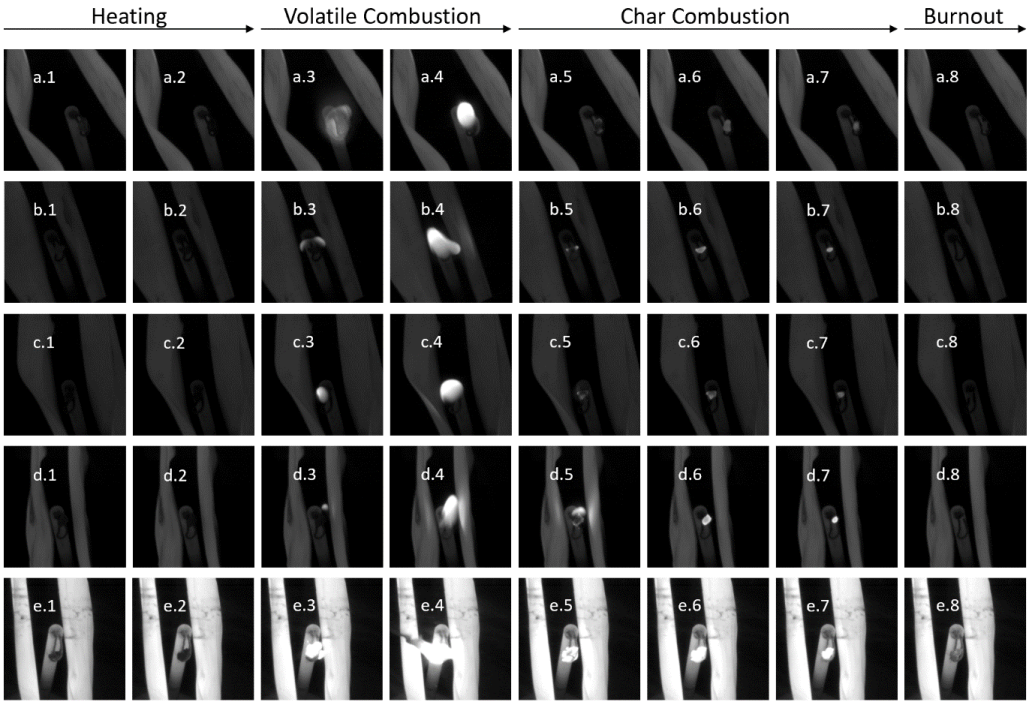

Figure 4.1 Representative high-speed cinematography frames of combustion processes of raw and torrefied single particle fuels (a: olive residue, b: almond shell, c: torrefied olive residue, d: torrefied almond shell, e: Tunçbilek lignite). Tunçbilek lignite sequence is shown for comparison purposes.

The high-speed cinematography frames from the combustion of individual chars obtained from slow and fast pyrolysis are presented in Figure 4.2 and Figure 4.3. Both slow and fast pyrolyzed fuels presented similar qualitative combustion behavior. Firstly, the char underwent surface ignition, followed by char combustion.

OR and AS chars became a quasi-spherical shape after combustion due to bridge-breaking and subsequent fluidization and/or partial ash melting. On the other hand, TL char remained in its original shape. Even though some residual volatiles might have been present, particularly in the chars from fast pyrolysis, the combustion of these volatiles was not notoriously identified. As previously stated by Howard and Essenhigh [98], when the particle diameter was below a certain threshold, the volatile flame did not detach from the particle surface, and the volatiles and char burned simultaneously on the surface of the particle, and observations herein suggested a similar critical diameter threshold for the biochars. Differences in the combustion of chars from slow and fast pyrolysis will be examined quantitatively in the subsequent subsections.

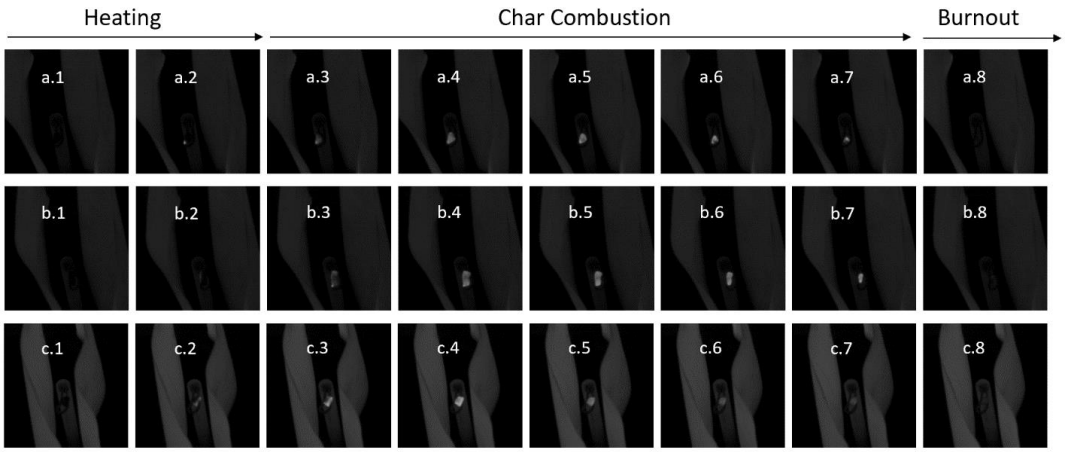

Figure 4.2 Representative high-speed cinematography frames of combustion processes of fast pyrolyzed single particle fuels (a: olive residue char – OR-H, b: almond shell char – AS-H, c: Tunçbilek lignite char – TL-H).

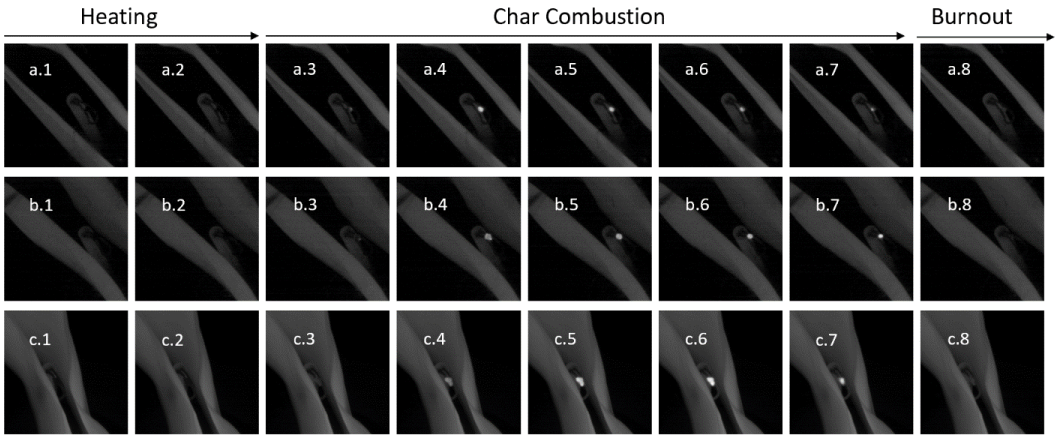

Figure 4.3 Representative high-speed cinematography frames of combustion processes of slow pyrolyzed single particles fuels (a: olive residue char – OR-L, b: almond shell char – AS-L, c: Tunçbilek lignite char – TL-L).

4.2 Ignition Delay Time

The ignition delay times of all OR, AS and TL with their pre-treatments are presented in Figure 4.4, Figure 4.5, and Figure 4.6, respectively. It can be depicted from the figures that no correlation was observed between the particle mass and the ignition delay time except for chars obtained from slow pyrolysis. Since there was no volatile left in the slow pyrolyzed particles, char ignition occurs; therefore, the ignition delay time was strongly dependent on the particle mass. On the other hand, ignition was partially dependent on mass for fast pyrolyzed chars since there might be residual volatiles. Even though a surface ignition mode was observed for both slow and fast pyrolysis chars, the decrease in the ignition delay time of the fast pyrolyzed chars is most likely due to the presence of a burning volatile cloud attached to the surface of fast pyrolysis chars and/or the higher porosity of the fast pyrolysis chars. To better understand the influence of pre-treatment on the ignition delay time of the fuels, 2 mg fuels were selected, and the ignition delay times averaged and plotted as shown in Figure 4.7. The ignition delay time of TL was shorter than both raw OR and AS. The effect of torrefaction on the ignition delay times was different in OR and AS;

the delay time increased for OR-T (+ ~2 s) while it decreased for AS-T (- ~2.5 s) (see Figure 4.4, Figure 4.5, Figure 4.6, and Figure 4.7). The ignition delay time of slow pyrolyzed fuels was significantly longer than all other pre-treated and raw fuels. During fast pyrolysis, macropores and accessible carbon sites are created due to the increasing pressure of volatiles inside the particle, leading to rapid release of the volatiles. Moreover, the extensive bridge-breaking during pyrolysis was not followed by cross-linking of the char due to insufficient residence time, and as a result, highly porous particles are formed [99]. During slow pyrolysis, the volatiles are removed slowly and completely, and the particles withstand heating and cooling cycles for longer periods of time that allow for cross-linking of the char and result in a more stable carbon structure and higher carbon content (see Table 2) that may also undergo thermal annealing at high temperatures.

As noticed from Figure 4.4, Figure 4.5, and Figure 4.6, the ignition delay times of slow pyrolyzed fuel particles are scattered, compared to other fuels. These scattered data appear due to other heterogeneities such as hot spots, non-uniform char structure (high and low porosity among the same fuel particle), different chemical compositions, and increasing moisture content.

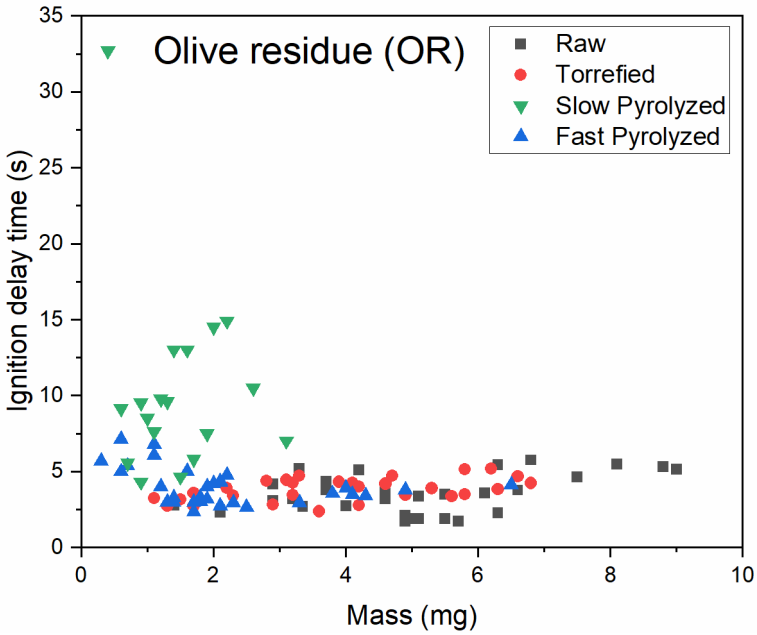

Figure 4.4 Ignition delay times for OR, OR-T, OR-L and OR-H

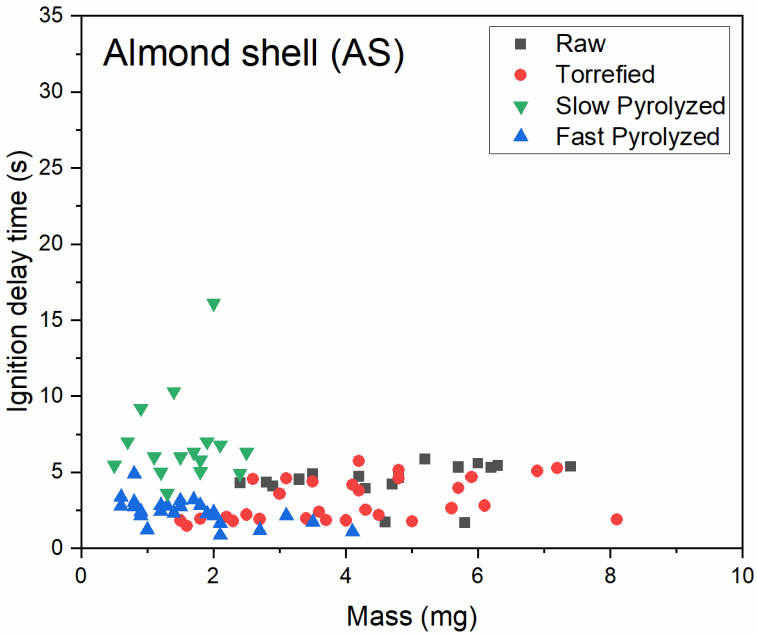

Figure 4.5 Ignition delay times for AS, AS-T, AS-L and AS-H

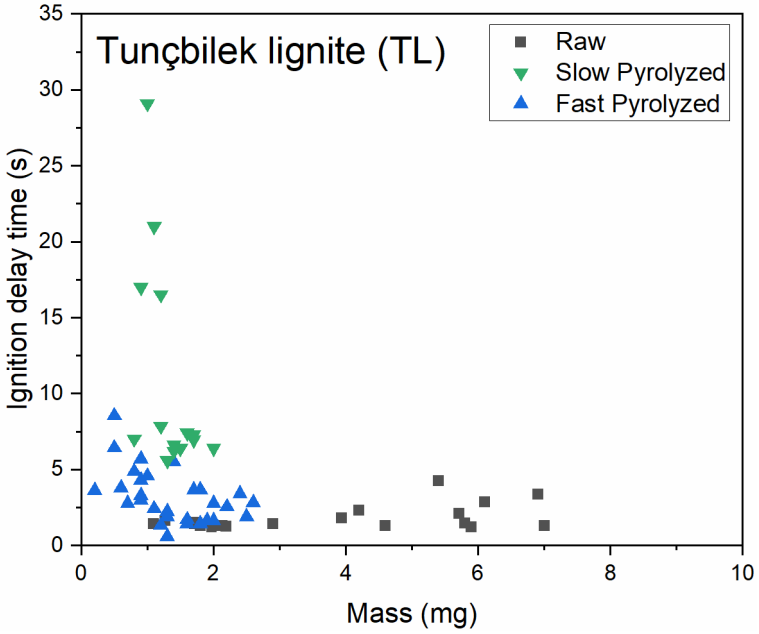

Figure 4.6 Ignition delay times for TL, TL-L and TL-H

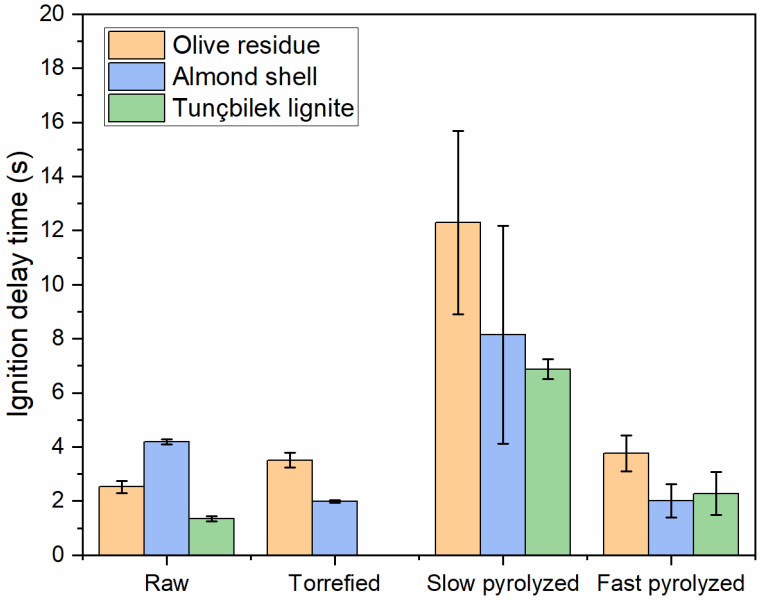

Figure 4.7 Ignition delay times for selected particles with 2 (+/- 0.2) mg with standard deviation.

4.3 Volatile and Char Combustion Times

The recorded videos were analyzed, and the correlated times were recorded in order to comprehend the effect of pre-treatment methods on the combustion times. All particles were weighed to establish empirical correlations between the burnout time and particle size/mass. The comparison of the total burnout, volatile combustion, and char combustion times is an indicative method for analyzing the discrepancies between different fuel particle combustion, as the heat transfer and combustion behavior may differ for each fuel. Since the experimental device's heat transfer and combustion conditions deviate from the actual boiler conditions, the volatile and char combustion times cannot be directly correlated with the ones from actual applications. This analysis can be used to compare the fuels.

4.3.1 Effect of Fuel Type

The raw fuels and their pre-treated particles were analyzed for their volatile and char combustion times. The volatile combustion times of the particles with the tendency line are plotted in Figure 4.8. The char combustion times of the OR, AS, and TL with the tendency line are plotted in Figure 4.9, Figure 4.10, and Figure 4.11, respectively.

The volatile combustion times of Tunçbilek lignite particles (TL) were similar to those of biomass raw and torrefied fuels (1-3 seconds in 1-9 mg fuel masses) even the TL volatile matter content is 40% less than the torrefied and raw biomass (see Table 2), as shown in Figure 4.8. This depicts that devolatilization rate and/or combustion of TL volatiles were lower since they consisted of heavier hydrocarbons with lower diffusivity in the air [30]. The volatile combustion times of torrefied biomass were comparable to those from the raw biomass, with a difference of 0.4 seconds, as shown in Figure 4.8. In the same way, Panahi et al. [71] also reported a small difference in volatile combustion times for raw and torrefied biomass fuels with different particle sizes in that study.

Char combustion times were also reported for all fuels in Figure 4.9, Figure 4.10, and Figure 4.11. As shown in the figures, the char combustion times of pre-treated fuels were remarkably increased compared to raw fuels. The average char combustion time over all particle masses was increased by ~2.5 s for torrefied fuels compared to that of raw biomass fuels. This increase in char combustion times was expected since the fuel's volatile and moisture content decreases with torrefaction. For the raw fuels, the char combustion time of TL was higher than the biomass by ~10s when the fuel particles of the same mass were considered over all the mass range. This difference was expected since the fixed carbon in TL is significantly more than biomass fuels. The R-square values of the combustion times of the fuels are presented in Table 3. The R-square values for Section 4.3.1 and Section 4.3.2 are the same since Section 4.3.1 uses the mass of the fuel, and Section 4.3.2 uses the normalized masses. As noticed from Table 3, the raw Tunçbilek lignite volatile and char combustion times have the lowest R-square values compared to the other fuels since the data is scattered. As explained in Section 4.1, the volatile build-up during the heating phase results in swelling of the particles and causes the volatiles to come out as jets. During this phase and volatile combustion phase, in some particles, the volatile jet release may come out in different flow speeds, resulting in different volatile combustion times. Also, the volatile jet release may create larger porosities on the particle structure, and as a result, the number of active carbon sites on the fuel particles may increase. This difference in Tunçbilek lignite particles' structure results in different char combustion times.

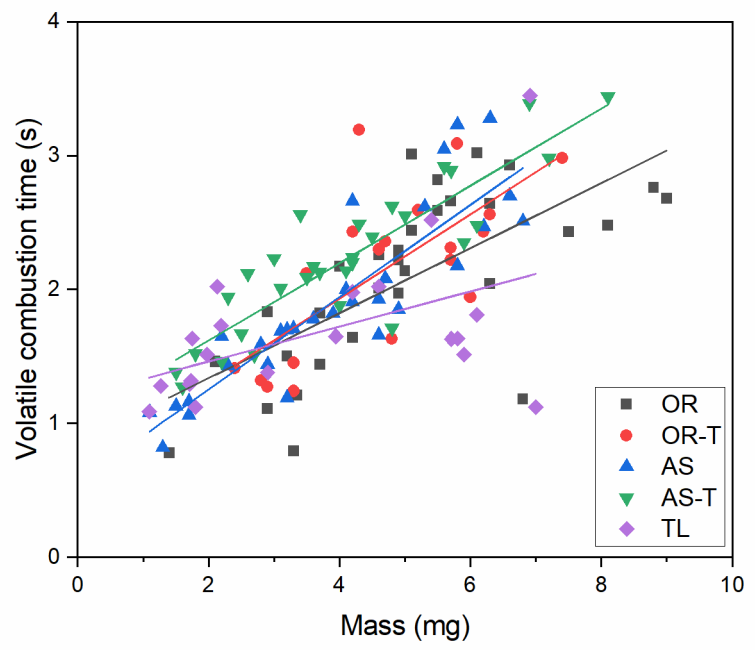

Figure 4.8 Volatile combustion times for all raw and torrefied fuels studied. Lines represent linear fit.

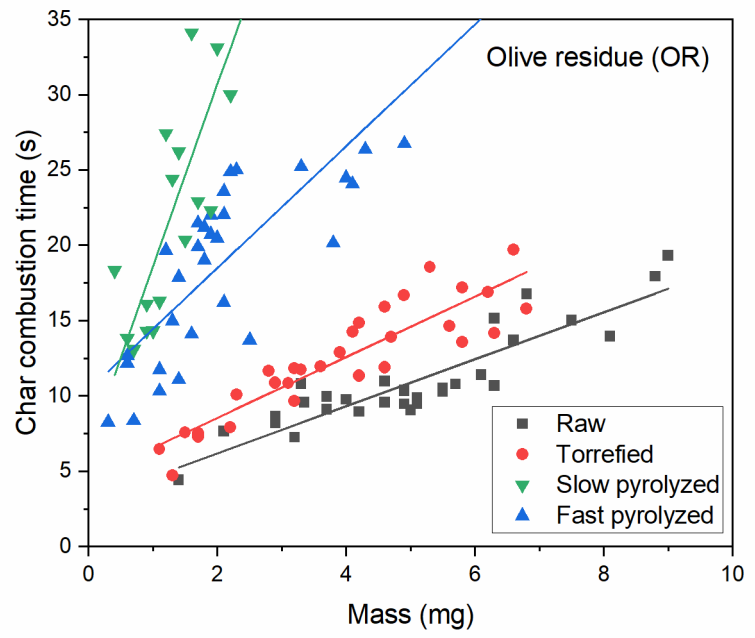

Figure 4.9 Char combustion times for all olive residue studied. Lines represent linear fit.

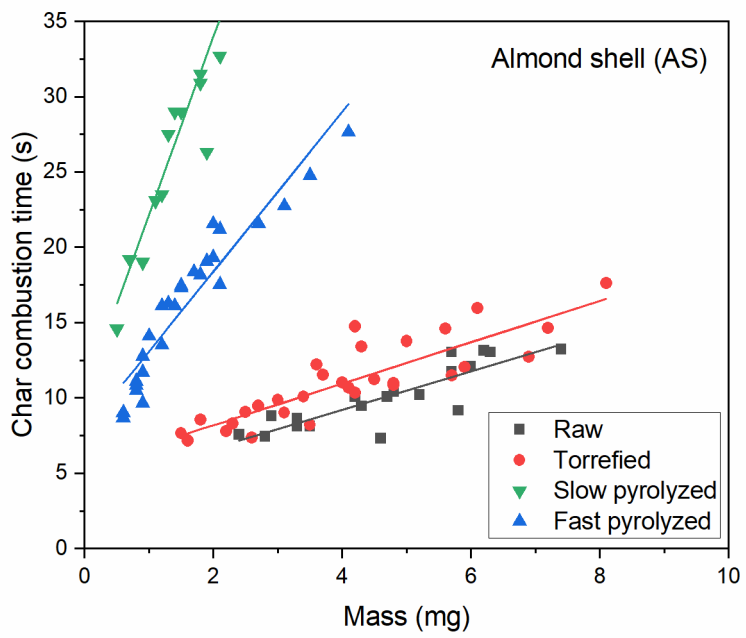

Figure 4.10 Char combustion times for all almond shell studied. Lines represent linear fit.

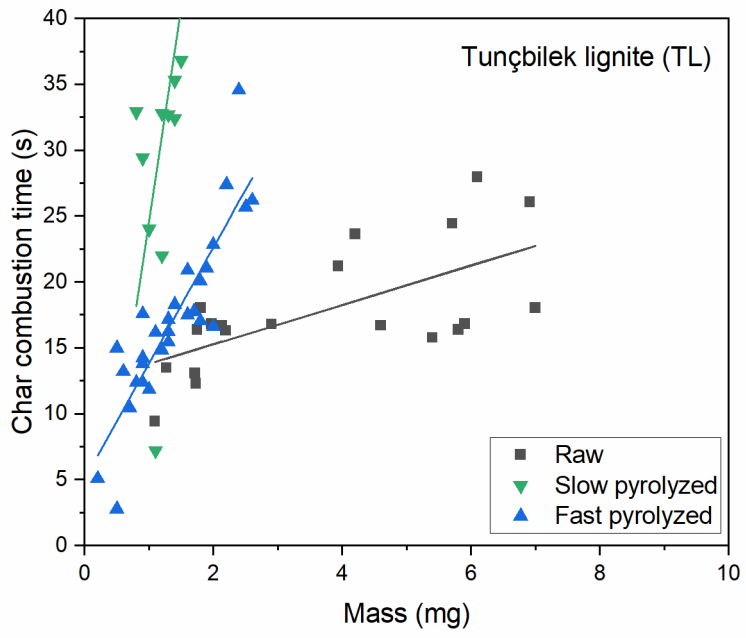

Figure 4.11 Char combustion times for all Tunçbilek lignite studied. Lines represent linear fit.

Table 3. R-Square Values for Combustion Times of the Fuels

Fuel	R-Square	
	Volatile Combustion	Char Combustion
OR	0.45965	0.79929
OR-T	0.47352	0.80831
OR-H	-	0.69437
OR-L	-	0.77765
AS	0.76761	0.72443
AS-T	0.76688	0.73528
AS-H	-	0.88931
AS-L	-	0.83421
TL	0.1975	0.39955
TL-H	-	0.76008
TL-L	-	0.58529

In Table 2, it can be noticed that the fixed carbon content is increased with every pre-treatment method. Since char combustion mainly burns the fixed carbon inside the char structure, an increase in char combustion times was expected. The most severe char combustion time difference with increasing particle mass is in slow pyrolyzed fuels since the fixed carbon content percentage is the highest in slow pyrolyzed fuels (see Table 2).

Moreover, as noticed from the figures, tendency line slopes are increasing with the pre-treatment methods. This slope increase can also be explained by increasing fixed carbon content. Since the fixed carbon content percentage is higher in pre-treated fuels, the change in the amount of fixed carbon inside a fuel particle increases per mass change. The lowest slope increase was observed in torrefied fuels, and the highest slope increase was observed in slow pyrolyzed fuels. This was expected due to torrefied fuels and slow pyrolyzed fuels having the lowest and highest fixed carbon content amongst the pre-treated, respectively (see Table 2). Even though the char combustion time increase and tendency line slope increase can be explained by

the increasing fixed carbon content, the effect of pre-treatments must be discussed in detail in order to see how the combustion times are affected.

4.3.2 Effect of Thermal Pre-treatment

In order to comprehend the effect of thermal pre-treatments, each particle mass is normalized with their volatile matter and fixed carbon content to see how the combustion times are affected when there is the same amount of volatile and fixed carbon matter. Each particle's volatile and char combustion times were outlined in Figure 4.13, Figure 4.14, Figure 4.15, and Figure 4.16, based on the mass of particle’s volatile matter and fixed carbon content. The volatile and char mass of the particles were calculated using the proximate analysis results in Table 2.

In Figure 4.12, it is seen that when the same volatile matter mass is considered, the torrefaction process slightly increased the volatile combustion time of both OR and AS; however, the volatile combustion time of the TL was still longer than the raw and torrefied fuels of OR and AS. The volatile combustion time of TL was longer by ~0.2 s compared to AS-T and ~1 s compared to OR-T. This further depicts the lower devolatilization and volatile combustion rates from Tunçbilek lignite as the same volatile mass particles were compared. As shown in Figure 4.12, torrefaction increased the tendency line slope of OR particles. On the other hand, the tendency line slope of AS particles is decreased with torrefaction. It shows that the torrefaction increases the devolatilization rate of larger OR particles. However, it decreases the devolatilization rate of larger AS particles.

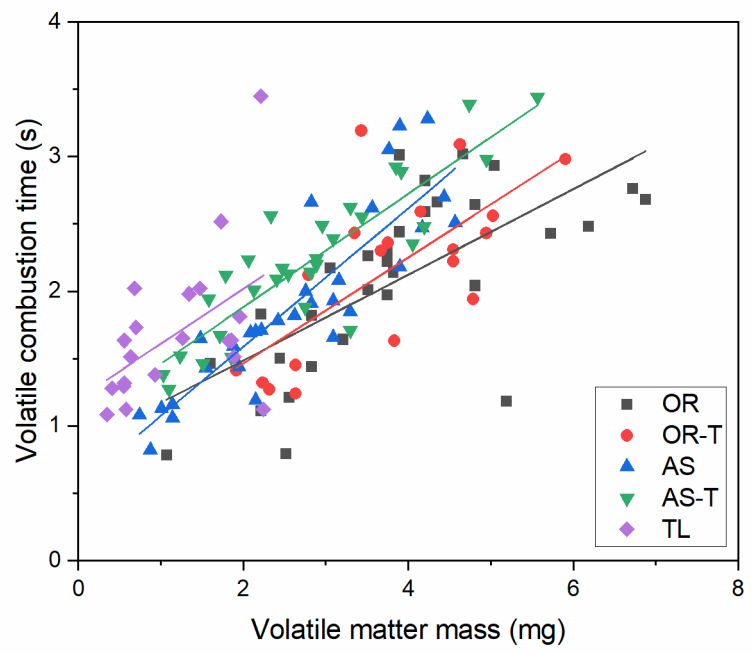

Figure 4.12 Volatile combustion times for all raw and torrefied fuels studied versus volatile matter content of the fuels. Lines represent linear fit.

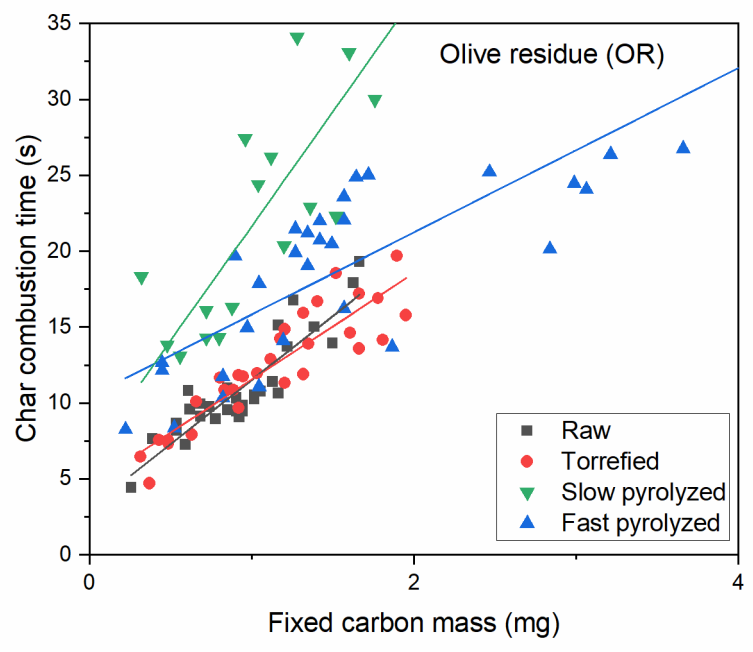

Figure 4.13 Char combustion times for all fuels studied versus fixed carbon content of OR fuels. Lines represent linear fit.

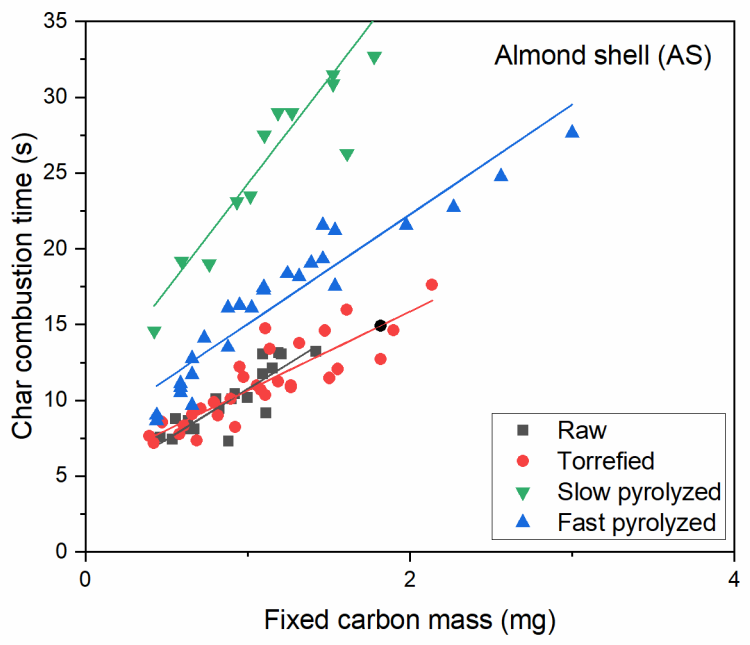

Figure 4.14 Char combustion times for all fuels studied versus fixed carbon content of AS fuels. Lines represent linear fit.

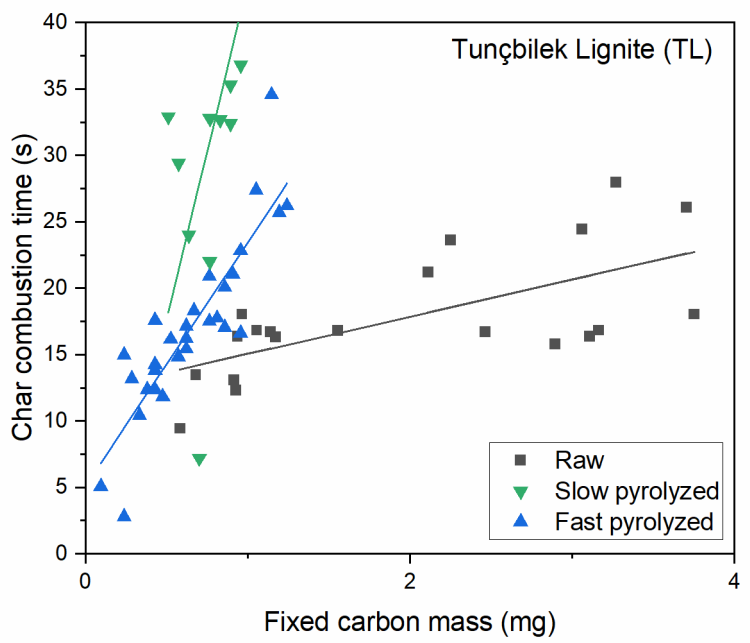

Figure 4.15 Char combustion times for all fuels studied versus fixed carbon content of TL fuels. Lines represent linear fit.

Fixed carbon content influences char combustion time for all fuels. However, other parameters such as porosity, fuel homogeneity, shape, size, chemical composition, and molecular structure can also affect the burning times. In Figure 4.13, Figure 4.14, and Figure 4.15, it is noticeable that even with the same fixed carbon amount considered for all fuels, the pre-treatment methods influence char combustion time.

It is noticeable that in Table 3 and Figure 4.12, the R-square values of OR, OR-T, and TL are low compared to AS and AS-T, resulting in more scattered data. This depicts that the volatile combustion times depend not only on the volatile matter mass but also on the particle morphology and heterogeneities among the fuels. As explained in Section 4.3.1, the structure change during the heating phase and differences in volatile release in TL may be the reason behind this scattering. Moreover, scattering in OR and OR-T may be due to heterogeneity of the fuel. OR may include more olive stones or more dust changing in the same fuel set, resulting in different volatile release conditions. Same with Section 4.3.1, the R-square value of TL for char combustion times in Figure 4.15 is lower than fast and slow pyrolyzed TL. Again, this difference can be explained by the resulting particle morphology of the TL particles after the heating and devolatilization phase.

As noticed from the figures, when the same fixed carbon mass is considered, the slow pyrolyzed fuels had the highest char combustion times for all the fuels. Fast pyrolysis also increased the char combustion times; however, the effect was not as impactive as slow pyrolysis. To see the impact in detail, the same fixed carbon mass range should be investigated.

Particles containing 1 mg fixed carbon were selected to clearly depict the influence of thermal pre-treatment methods on char combustion times and shown in Figure 4.16. For the same fixed carbon amount, pre-treatment increased the char combustion time by ~5s for fast pyrolyzed biomass fuels, ~10 s for fast pyrolyzed TL, ~15 s for slow pyrolyzed biomass fuels and ~30 s for slow pyrolyzed TL. This increase can be explained with the same approach as discussed in Section 4.2. Due to the rapid increase in temperature, the volatiles is released rapidly. Hence,

macropores and accessible carbon sites are created. Furthermore, cross-linking of the char was not happening due to insufficient residence time after the extensive bridge-breaking, resulting in highly porous particles [99]. Having insufficient time makes the inorganic matter inside the fuels not affect cross-linking since the bonds are breaking fast at very high heating rates [43]. During slow pyrolysis, since the volatiles are removed slowly and completely, the particles withstand heating and cooling cycles for long periods of time, allowing the chars to cross-link. Hence, more stable carbon structured and higher carbon content fuels are produced. During the period, particles may also undergo thermal annealing at high temperatures.

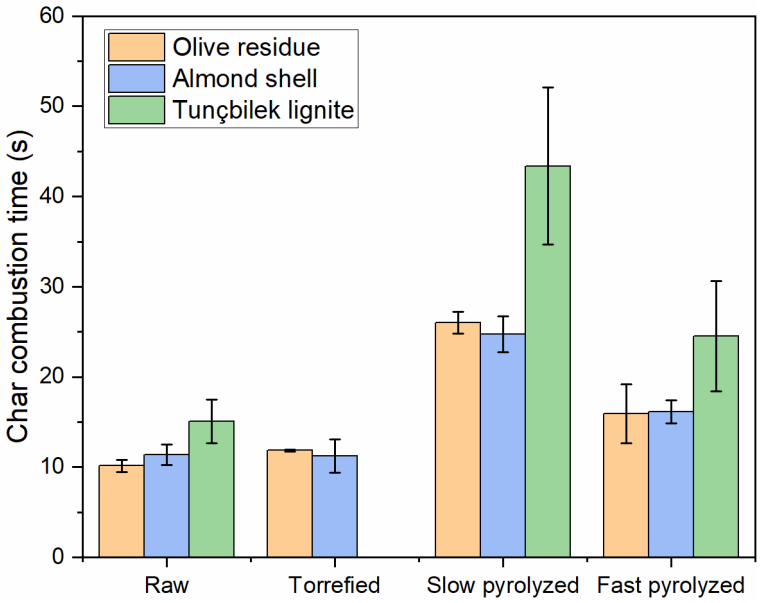

Figure 4.16 Char combustion times for selected particles with 1 (+/- 0.2) mg fixed carbon for all studied fuels with standard deviation. Values for raw fuels displayed for comparison purposes.

4.4 Burnout Time

The burnout time is the sum of volatile and char combustion time for all fuels, except chars. For the latter, the char combustion time is equal to the burnout time. The volatile combustion time of OR and AS was around 18% of the total burnout time

while the volatile combustion time of TL was around 10%. Total burnout times for selected 2 mg fuels are shown in Figure 4.17. Olive residue and almond shell chars produced from fast pyrolysis had similar burnout (~20 s) times compared to raw Tunçbilek lignite. This depicts the potential of co-firing raw TL with fast pyrolyzed OR and AS in the existing power plants. Due to the heterogeneity of the biomass fuels, the size and content of the olive residue and almond shell particles for the same mass can vary. Hence, it is hard to attribute precise burnout time for the olive residue and almond shell for the same particle mass.

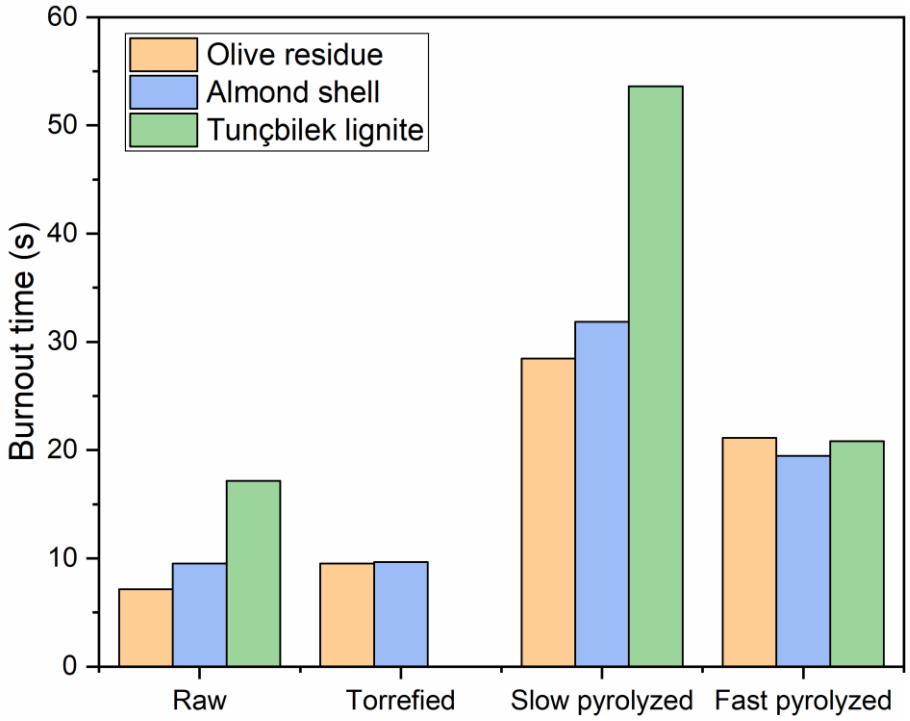

Figure 4.17 Burnout times for selected particles with 2 (+/- 0.2) mg mass, for all studied fuels

The shape of the particles can also have an influence on the total burnout time. The aspect ratio was calculated for each fuel particle by dividing major length by minor length. However, no significant effect of aspect ratio was observed on the ignition

delay, volatile combustion, char combustion, and burnout times. Results for the raw fuels and olive residue fuels are shown in Figure 4.18 and Figure 4.19, respectively.

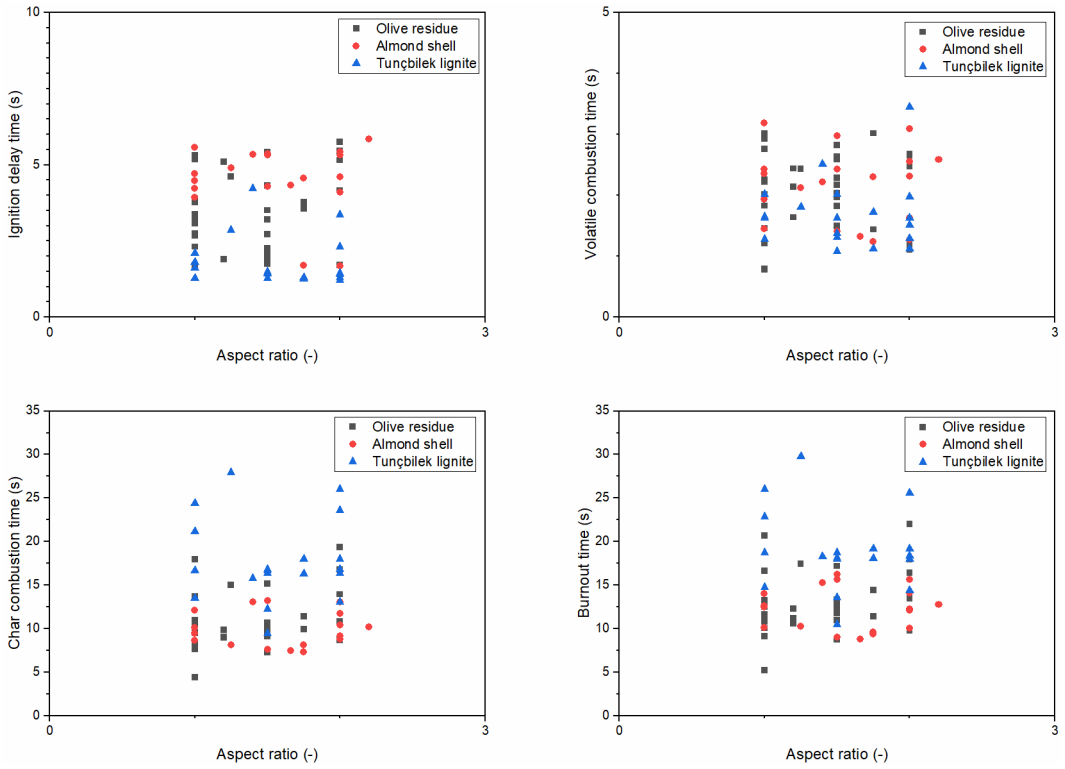

Figure 4.18 Ignition delay time, volatile combustion time, char combustion time, and burnout combustion time as a function of the particle aspect ratio for all raw fuels studied.

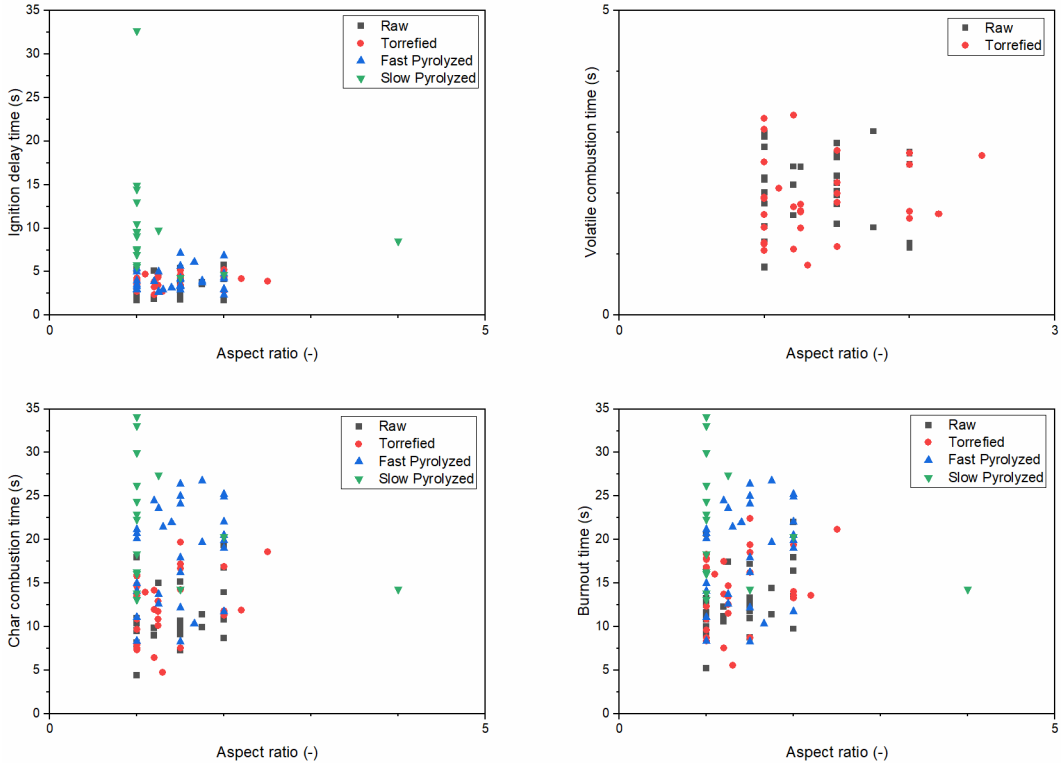

Figure 4.19 Ignition delay time, volatile combustion time, char combustion time, and burnout combustion time as a function of the particle aspect ratio for olive residue in raw, torrefied, slow pyrolyzed, and fast pyrolyzed form.

CHAPTER 5

CONCLUSION AND FUTURE WORKS

5.1 Conclusion

This study focuses on the effect of particle mass, size and thermochemical pre-treatment techniques (torrefaction and pyrolysis) on the combustion modes and times of single biomass and lignite particles. During the experiments, the following results have been achieved:

- During the combustion of Tunçbilek lignite, soot release was observed while devolatilization and swelling were observed during the ignition delay phase, depicting Tunçbilek lignite burning behavior resembled bituminous coal combustion.
- All raw and torrefied fuels were ignited in the gas phase. Following ignition, two-phase combustion was observed for these fuels. On the other hand, chars produced from either slow or fast pyrolysis had a surface ignition.
- During the experiments, it is observed that the particle mass and size did not affect the ignition delay time.
- Heavier hydrocarbon content of Tunçbilek lignite resulted in longer volatile combustion times than the biomass fuels, which are raw and torrefied when particles containing the same amount of volatile matter were compared since the volatiles in Tunçbilek lignite were composed of heavier hydrocarbons with lower diffusivity in the air.
- The volatile combustion flame of biomass, raw and torrefied fuels were bright and spherical, where the flame of Tunçbilek lignite was jet. This is due to the different porosity levels of biomass and lignite fuels.
- During biomass char combustion, partial melting due to the surface tension was observed; however, Tunçbilek lignite preserved its inordinate shape.

- Increasing particle mass increased burnout times of all fuels.
- Compared to raw fuels, slow pyrolysis increased the burnout times of all fuels by ~20s for biomass and ~40s for Tunçbilek lignite. Fast pyrolysis increased the burnout times of olive residue and almond shell biomass fuels, ~13s for olive residue and ~11s for the almond shell, but did not significantly affect those of Tunçbilek lignite.
- Olive residue and almond shell chars produced from fast pyrolysis had similar burnout times (~20s) compared to raw Tunçbilek lignite (~19s). This depicts the potential of co-firing raw Tunçbilek lignite with olive residue and almond shell chars from fast pyrolysis in the existing power plants.

This study concludes that the fast pyrolyzed olive residue and almond shell can be used in a powerplant that is operated with Tunçbilek lignite. Even though the announced fuels can be co-fired in already operating power plants that use Tunçbilek lignite, it is only announced by investigating their combustion times. Hence, further research must be done to know the optimum combustion conditions (such as blending rate, bed temperature, air-fuel ratio) and the investment required to operate such a powerplant. Moreover, the parameters that are affecting slagging, fouling and agglomeration must be investigated in order to see whether the fast pyrolyzed olive residue and almond shell fuels are proper to use in an operating power plant.

5.2 Future Works

As future research, not only olive residue, almond shell and Tunçbilek lignite, but also other different types of biomasses such as wood chips, sugar cane, hazelnut shell can be used in experiments. Also, besides the Tunçbilek lignite, other widely used lignites (i.e., Soma lignite and Afşin-Elbistan lignite) can be used to decide further which biomass fuel can be co-fired with lignite in Turkey.

To further understand the effect of the pre-treatment methods, different conditions could be used. Changing the pre-treatment conditions would let us choose the

optimum environment to use the biomass fuels in the power plants, co-firing with lignite.

Moreover, different plateau temperatures and heating rates can be set for the single-particle combustion experiments. Different temperatures and heating rates would allow the observation of how the ignition and combustion modes times would be influenced. As a result, the correlation between combustion times, heating rate, and operating temperature would be investigated. Conducting this experimental methodology with different parameters would yield valuable data for us to understand the behavior of biomass fuels to use them to generate cleaner energy for the future.

REFERENCES

[1] IEA. Bioenergy - 2020. n.d.

[2] Ministry of Energy and Natural Resources of Turkey. Energy Balance Report. 2015.

[3] Ministry of Energy and Natural Resources of Turkey. Energy Balance Report. 2018.

[4] Eksi G, Karaosmanoglu F. Combined bioheat and biopower: A technology review and an assessment for Turkey. Renew Sustain Energy Rev 2017;73:1313–32. https://doi.org/10.1016/j.rser.2017.01.093.

[5] Koppejan J. The Handbook of Biomass Combustion and Cofiring The Handbook of Biomass Combustion and Co-firing Edited by Sjaak van Loo and Jaap Koppejan 2016.

[6] Saidur R, Abdelaziz EA, Demirbas A, Hossain MS, Mekhilef S. A review on biomass as a fuel for boilers. Renew Sustain Energy Rev 2011;15:2262–89. https://doi.org/10.1016/j.rser.2011.02.015.

[7] Gustavsson L, Johansson B. Cogeneration: One way to use biomass efficiently. Heat Recover Syst CHP 1994;14:117–27. https://doi.org/10.1016/0890-4332(94)90003-5.

[8] Wiltsee G. Lessons Learned from Existing Biomass Power Plants 2000.

[9] McGowan TF, Brown ML, Bulpitt WS, Walsh Jr. JL. Biomass and Alternate Fuel Systems: An Engineering and Economic Guide. n.d.

[10] Sami M, Annamalai K, Wooldridge M. Co-firing of coal and biomass fuel blends. Prog Energy Combust Sci 2001;27:171–214. https://doi.org/10.1016/S0360-1285(00)00020-4.

[11] Dayton D. A Summary of NO x Emissions Reduction from Biomass Cofiring 2002:7.

[12] Khan AA, de Jong W, Jansens PJ, Spliethoff H. Biomass combustion in fluidized bed boilers: Potential problems and remedies. Fuel Process Technol 2009;90:21–50. https://doi.org/10.1016/j.fuproc.2008.07.012.

[13] Demirbas A. Potential applications of renewable energy sources, biomass combustion problems in boiler power systems and combustion related environmental issues. Prog Energy Combust Sci 2005;31:171–92. https://doi.org/10.1016/j.pecs.2005.02.002.

[14] Demirbas A. Petroleum Refinery and Biorefinery 2010.

[15] Niu Y, Tan H, Hui S. Ash-related issues during biomass combustion: Alkali-induced slagging, silicate melt-induced slagging (ash fusion), agglomeration, corrosion, ash utilization, and related countermeasures. Prog Energy Combust Sci 2016;52:1–61. https://doi.org/10.1016/j.pecs.2015.09.003.

[16] Rosillo-Calle F, Hemstock S, de Groot P, Woods J. The Biomass Assessment Handbook. Bioenergy for a sustainable development. 2007.

[17] Capehart BL. Encyclopedia of energy engineering and technology. vol. 45. 2008. https://doi.org/10.5860/choice.45-2362.

[18] Nunes LJR, Matias JCO, Catalão JPS. Biomass combustion systems: A review on the physical and chemical properties of the ashes. Renew Sustain Energy Rev 2016;53:235–42. https://doi.org/10.1016/j.rser.2015.08.053.

[19] McIlveen-Wright DR, Huang Y, Rezvani S, Wang Y. A technical and environmental analysis of co-combustion of coal and biomass in fluidised bed technologies. Fuel 2007;86:2032–42. https://doi.org/10.1016/j.fuel.2007.02.011.

[20] IEA. World Energy Balances: Overview - 2020. n.d.

[21] Özer B. A study on coal combustion: experiments and modelling. Middle East Technical University, 2019.

[22] U.S. Energy Information Administration. Coal explained. 2020.

[23] National Geographic. Coal n.d.

[24] Ward CR, Suárez-Ruiz I. Introduction to Applied Coal Petrology. Appl Coal Petrol 2008:1–18. https://doi.org/10.1016/B978-0-08-045051-3.00001-4.

[25] Borja R, De I, Csic G. 2.55 - Biogas Production. vol. 1. Second Edi. Elsevier B.V.; 2011. https://doi.org/10.1016/B978-0-08-088504-9.00126-4.

[26] Mutlu B. Hybridization of Single Flash Geothermal Power Plant with Biomass Driven SCO2 Topping Cycle. Middle East Technical University, 2020.

[27] Suresh NS, Thirumalai NC, Dasappa S. Modeling and analysis of solar thermal and biomass hybrid power plants. Appl Therm Eng 2019;160:114121. https://doi.org/10.1016/j.applthermaleng.2019.114121.

[28] Lavoisier A. Homogeneous and heterogeneous combustion n.d.;V:413–30.

[29] Levendis YA, Joshi K, Khatami R, Sarofim AF. Combustion behavior in air of single particles from three different coal ranks and from sugarcane bagasse. Combust Flame 2011;158:452–65. https://doi.org/10.1016/j.combustflame.2010.09.007.

[30] Magalhães D, Panahi A, Kazanç F, Levendis YA. Comparison of single particle combustion behaviours of raw and torrefied biomass with Turkish lignites. Fuel 2019;241:1085–94. https://doi.org/10.1016/j.fuel.2018.12.124.

[31] Taylor P, Saito M, Sadakata M, Saka T. Combustion Science and Technology Measurements of Surface Combustion Rate of Single Coal Particles in Laminar Flow Furnace 2015:37–41. https://doi.org/10.1080/00102208708960319.

[32] Tomeczek J. Coal Combustion. United States: 1992.

[33] Toporov DD. Combustion of Pulverised Coal in a Mixture of Oxygen and Recycled Flue Gas. n.d.

[34] Kan T, Strezov V, Evans TJ. Lignocellulosic biomass pyrolysis: A review of product properties and effects of pyrolysis parameters. Renew Sustain Energy Rev 2016;57:1126–40. https://doi.org/10.1016/j.rser.2015.12.185.

[35] Meier D, Van De Beld B, Bridgwater A V., Elliott DC, Oasmaa A, Preto F. State-of-the-art of fast pyrolysis in IEA bioenergy member countries. Renew Sustain Energy Rev 2013;20:619–41. https://doi.org/10.1016/j.rser.2012.11.061.

[36] Debiagi P, Gentile G, Cuoci A, Frassoldati A, Ranzi E, Faravelli T. A predictive model of biochar formation and characterization. J Anal Appl Pyrolysis 2018. https://doi.org/10.1016/j.jaap.2018.06.022.

[37] Safdari M, Amini E, Weise DR, Fletcher TH. Heating rate and temperature e ff ects on pyrolysis products from live wildland fuels ☆. Fuel 2019;242:295–304. https://doi.org/10.1016/j.fuel.2019.01.040.

[38] Wang B, Xu F, Zong P, Zhang J, Tian Y, Qiao Y. Effects of heating rate on fast pyrolysis behavior and product distribution of Jerusalem artichoke stalk by using TG-FTIR and Py-GC / MS. Renew Energy 2019;132:486–96. https://doi.org/10.1016/j.renene.2018.08.021.

[39] Howard JB, Essenhigh RH. Pyrolysis of coal particles in pulverized fuel flames 1967.

[40] Jayaraman K, Gökalp I. Pyrolysis , combustion and gasification characteristics of miscanthus and sewage sludge. ENERGY Convers Manag 2015;89:83–91. https://doi.org/10.1016/j.enconman.2014.09.058.

[41] Seo DK, Park SS, Kim YT, Hwang J, Yu T. Study of coal pyrolysis by thermo-gravimetric analysis (TGA) and concentration measurements of the

evolved species. J Anal Appl Pyrolysis 2011;92:209–16. https://doi.org/10.1016/j.jaap.2011.05.012.

[42] Jayaraman K, Gokalp I, Bostyn S. High ash coal pyrolysis at different heating rates to analyze its char structure, kinetics and evolved species. J Anal Appl Pyrolysis 2015. https://doi.org/10.1016/j.jaap.2015.03.007.

[43] Trubetskaya A, Jensen PA, Jensen AD, Garcia Llamas AD, Umeki K, Glarborg P. Effect of fast pyrolysis conditions on biomass solid residues at high temperatures. Fuel Process Technol 2016;143:118–29. https://doi.org/10.1016/j.fuproc.2015.11.002.

[44] Magalhães D, Gürel K, Matsakas L, Christakopoulos P, Pisano I, Leahy JJ, et al. Prediction of yields and composition of char from fast pyrolysis of commercial lignocellulosic materials, organosolv fractionated and torrefied olive stones. Fuel 2021;289:119862. https://doi.org/10.1016/j.fuel.2020.119862.

[45] Le Manquais K, Snape CE, Mcrobbie I, Barker J. Evaluating the Combustion Reactivity of Drop Tube Furnace and Thermogravimetric Analysis Coal Chars with a Selection of Metal Additives 2011:981–9.

[46] Farrow TS, Sun C, Snape CE. Impact of CO2 on biomass pyrolysis , nitrogen partitioning , and char combustion in a drop tube furnace. J Anal Appl Pyrolysis 2015;113:323–31. https://doi.org/10.1016/j.jaap.2015.02.013.

[47] Le Manquais K, Snape C, McRobbie I, Barker J, Pellegrin V. Comparison of the combustion reactivity of TGA and drop tube furnace chars from a bituminous coal. Energy and Fuels 2009;23:4269–77. https://doi.org/10.1021/ef900205d.

[48] Magalhães D. Investigation of Alternative Biomass Fuels and Turkish Lignites at High Heating Rate Pyrolysis and Combustion Conditions. Middle East Technical University, 2021.

[49] Collard F, Blin J. A review on pyrolysis of biomass constituents : Mechanisms and composition of the products obtained from the conversion of cellulose , hemicelluloses and lignin. Renew Sustain Energy Rev 2014;38:594–608. https://doi.org/10.1016/j.rser.2014.06.013.

[50] Fletcher, Thomas H. and Kerstein AR, Pugmire, Ronald J. and Grant DM. A Chemical Percolation Model for Devolatilization: Summary. J Chem Inf Model 2013;53:1689–99.

[51] Trubetskaya A, Jensen PA, Jensen AD, Steibel M, Spliethoff H, Glarborg P. Influence of fast pyrolysis conditions on yield and structural transformation of biomass chars. Fuel Process Technol 2015;140:205–14. https://doi.org/10.1016/j.fuproc.2015.08.034.

[52] Panahi A, Levendis YA, Vorobiev N, Schiemann M. Direct observations on the combustion characteristics of Miscanthus and Beechwood biomass including fusion and spherodization. Fuel Process Technol 2017;166:41–9. https://doi.org/10.1016/j.fuproc.2017.05.029.

[53] Nhuchhen DR, Afzal MT. HHV predicting correlations for torrefied biomass using proximate and ultimate analyses. Bioengineering 2017;4. https://doi.org/10.3390/bioengineering4010007.

[54] Bridgeman TG, Jones JM, Shield I, Williams PT. Torrefaction of reed canary grass, wheat straw and willow to enhance solid fuel qualities and combustion properties. Fuel 2008;87:844–56. https://doi.org/10.1016/j.fuel.2007.05.041.

[55] van der Stelt MJC, Gerhauser H, Kiel JHA, Ptasinski KJ. Biomass upgrading by torrefaction for the production of biofuels: A review. Biomass and Bioenergy 2011;35:3748–62. https://doi.org/10.1016/j.biombioe.2011.06.023.

[56] Colin B, Dirion JL, Arlabosse P, Salvador S. Quantification of the torrefaction effects on the grindability and the hygroscopicity of wood chips.

Fuel 2017;197:232–9. https://doi.org/10.1016/j.fuel.2017.02.028.

[57] Shao J, Cheng W, Zhu Y, Yang W, Fan J, Liu H, et al. Effects of Combined Torrefaction and Pelletization on Particulate Matter Emission from Biomass Pellet Combustion. Energy & Fuels 2019;33:8777–85. https://doi.org/10.1021/acs.energyfuels.9b01920.

[58] Yang W, Zhu Y, Cheng W, Sang H, Yang H, Chen H. Characteristics of particulate matter emitted from agricultural biomass combustion Characteristics of particulate matter emitted from agricultural biomass combustion 2017.

[59] Yani S, Gao X, Wu H. Emission of Inorganic PM 10 from the Combustion of Torre fi ed Biomass under Pulverized-Fuel Conditions 2014. https://doi.org/10.1021/ef5023237.

[60] Wang Q, Yao H, Yu D, Dai L, Xu M. Emission Behavior of Particulate Matter during Co-combustion of Coal and Biomass in a Drop Tube Furnace † 2007:513–6.

[61] Han J, Yu D, Yu X, Liu F, Wu J, Zeng X, et al. Effect of the torrefaction on the emission of PM 10 from combustion of rice husk and its blends with a lignite 2018;000:1–8. https://doi.org/10.1016/j.proci.2018.07.011.

[62] Wang X, Adeosun A, Hu Z, Xiao Z, Khatri D, Li T, et al. Effect of feedstock water leaching on ignition and PM 1 . 0 emission during biomass combustion in a flat-flame. Proc Combust Inst 2018;000:1–9. https://doi.org/10.1016/j.proci.2018.05.096.

[63] Riaza J, Khatami R, Levendis YA, Álvarez L, Gil M V., Pevida C, et al. Combustion of single biomass particles in air and in oxy-fuel conditions. Biomass and Bioenergy 2014;64:162–74. https://doi.org/10.1016/j.biombioe.2014.03.018.

[64] Riaza J, Gibbins J, Chalmers H. Ignition and combustion of single particles

of coal and biomass. Fuel 2017;202:650–5. https://doi.org/10.1016/j.fuel.2017.04.011.

[65] Riaza J, Ajmi M, Gibbins J, Chalmers H. Ignition and combustion of single particles of coal and biomass under O2 / CO2 atmospheres. Energy Procedia 2017;114:6067–73. https://doi.org/10.1016/j.egypro.2017.03.1743.

[66] Marek E, Wiątkowski B. Reprint of "experimental studies of single particle combustion in air and different oxy-fuel atmospheres." Appl Therm Eng 2015;74:61–8. https://doi.org/10.1016/j.applthermaleng.2014.05.026.

[67] Riaza J, Mason PE, Jones JM, Williams A, Gibbins J, Chalmers H. Shape and size transformations of biomass particles during combustion. Fuel 2020;261:116334. https://doi.org/10.1016/j.fuel.2019.116334.

[68] Mason PE, Darvell LI, Jones JM, Pourkashanian M, Williams A. Single particle flame-combustion studies on solid biomass fuels. Fuel 2015;151:21–30. https://doi.org/10.1016/j.fuel.2014.11.088.

[69] Mock C, Lee H, Choi S, Manovic V. Combustion Behavior of Relatively Large Pulverized Biomass Particles at Rapid Heating Rates. Energy and Fuels 2016;30:10809–22. https://doi.org/10.1021/acs.energyfuels.6b01457.

[70] Flower M, Gibbins J. A radiant heating wire mesh single-particle biomass combustion apparatus. Fuel 2009;88:2418–27. https://doi.org/10.1016/j.fuel.2009.02.036.

[71] Panahi A, Tarakcioglu M, Schiemann M, Delichatsios M, Levendis YA. On the particle sizing of torrefied biomass for co-firing with pulverized coal. Combust Flame 2018;194:72–84. https://doi.org/10.1016/j.combustflame.2018.04.014.

[72] Panahi A, Vorobiev N, Schiemann M, Tarakcioglu M, Delichatsios M, Levendis YA. Combustion details of raw and torrefied biomass fuel particles with individually-observed size, shape and mass. Combust Flame

2019;207:327–41. https://doi.org/10.1016/j.combustflame.2019.06.009.

[73] Vorobiev N, Becker A, Kruggel-Emden H, Panahi A, Levendis YA, Schiemann M. Particle shape and Stefan flow effects on the burning rate of torrefied biomass. Fuel 2017;210:107–20. https://doi.org/10.1016/j.fuel.2017.08.037.

[74] Panahi A, Toole N, Wang X, Levendis YA. On the minimum oxygen requirements for oxy-combustion of single particles of torrefied biomass. Combust Flame 2020;213:426–40. https://doi.org/10.1016/j.combustflame.2019.12.012.

[75] Magalhães D, Kazanç F, Ferreira A, Rabaçal M, Costa M. Ignition behavior of Turkish biomass and lignite fuels at low and high heating rates. Fuel 2017;207:154–64. https://doi.org/10.1016/j.fuel.2017.06.069.

[76] Lee H, Choi S. Volatile flame visualization of single pulverized fuel particles. Powder Technol 2018;333:353–63. https://doi.org/10.1016/j.powtec.2018.04.048.

[77] Schiemann M, Haarmann S, Vorobiev N. Char burning kinetics from imaging pyrometry: Particle shape effects. Fuel 2014;134:53–62. https://doi.org/10.1016/j.fuel.2014.05.049.

[78] Biagini E, Narducci P, Tognotti L. Size and structural characterization of lignin-cellulosic fuels after the rapid devolatilization. Fuel 2008;87:177–86. https://doi.org/10.1016/j.fuel.2007.04.010.

[79] Lei K, Ye B, Cao J, Zhang R, Liu D. Combustion characteristics of single particles from bituminous coal and pine sawdust in O2/N2, O2/CO2, and O2/H2O atmospheres. Energies 2017;10. https://doi.org/10.3390/en10111695.

[80] Simões G, Magalhães D, Rabaçal M, Costa M. Effect of gas temperature and oxygen concentration on single particle ignition behavior of biomass fuels.

Proc Combust Inst 2017;36:2235–42. https://doi.org/10.1016/j.proci.2016.06.102.

[81] Lu Z, Jian J, Arendt Jensen P, Wu H, Glarborg P. Impact of KCl impregnation on single particle combustion of wood and torrefied wood. Fuel 2017;206:684–9. https://doi.org/10.1016/j.fuel.2017.05.082.

[82] Carvalho A, Rabaçal M, Costa M, Alzueta MU, Abián M. Effects of potassium and calcium on the early stages of combustion of single biomass particles. Fuel 2017;209:787–94. https://doi.org/10.1016/j.fuel.2017.08.045.

[83] Shan L, Kong M, Bennet TD, Sarroza AC, Eastwick C, Sun D, et al. Studies on combustion behaviours of single biomass particles using a visualization method. Biomass and Bioenergy 2018;109:54–60. https://doi.org/10.1016/j.biombioe.2017.12.008.

[84] Panahi A, Tarakcioglu M, Schiemann M, Delichatsios M, Levendis YA. On the particle sizing of torrefied biomass for co-firing with pulverized coal. Combust Flame 2018;194:72–84. https://doi.org/10.1016/j.combustflame.2018.04.014.

[85] Mills S. Prospects for coal and clean coal technologies in Turkey. July 2014;44:2–109.

[86] IEA. Energy Policies of IEA Countries: Turkey. 2016.

[87] Mayoral MC, Izquierdo MT, Andrés JM, Rubio B. Different approaches to proximate analysis by thermogravimetry analysis. Thermochim Acta 2001;370:91–7. https://doi.org/10.1016/S0040-6031(00)00789-9.

[88] Friedl A, Padouvas E, Rotter H, Varmuza K. Prediction of heating values of biomass fuel from elemental composition. Anal Chim Acta 2005;544:191–8. https://doi.org/10.1016/j.aca.2005.01.041.

[89] Majumder AK, Jain R, Banerjee P, Barnwal JP. Development of a new proximate analysis based correlation to predict calorific value of coal. Fuel

2008;87:3077–81. https://doi.org/10.1016/j.fuel.2008.04.008.

[90] Ehsana A, Yilmazoglu MZ. Design and exergy analysis of a thermal power plant using different types of Turkish lignite. Int J Thermodyn 2011;14:125–33. https://doi.org/10.5541/ijot.288.

[91] Amirabedin E, Yilmazoğlu MZ, Başkaya Ş. Exergetic evaluation of an integrated gasification combined cycle power plant simulated by seven different types of Turkish lignite. Turkish J Eng Environ Sci 2013;37:42–55. https://doi.org/10.3906/muh-1109-9.

[92] Akın SŞ, Magalhães D, Kazanç F. A study on the effects of various combustion parameters on the mineral composition of Tunçbilek fly ash. Fuel 2020;275. https://doi.org/10.1016/j.fuel.2020.117881.

[93] Furnaces P. Tubular Furnaces - PTF Series n.d. http://www.alserteknik.com/tüp-fırınlar/ptf-serisi.

[94] Mammadbaghir Baghirzade. Investigation of Turkish Lignites and Biomass at High Heating Rates by using Wire Mesh Apparatus. Middle East Technical University, 2018.

[95] Gil M V., Riaza J, Álvarez L, Pevida C, Rubiera F. Biomass devolatilization at high temperature under N2 and CO2: Char morphology and reactivity. Energy 2015;91:655–62. https://doi.org/10.1016/j.energy.2015.08.074.

[96] Gil M V., Riaza J, Álvarez L, Pevida C, Pis JJ, Rubiera F. Oxy-fuel combustion kinetics and morphology of coal chars obtained in N2 and CO2 atmospheres in an entrained flow reactor. Appl Energy 2012;91:67–74. https://doi.org/10.1016/j.apenergy.2011.09.017.

[97] Khatami R, Levendis YA. An overview of coal rank influence on ignition and combustion phenomena at the particle level. Combust Flame 2016;164:22–34. https://doi.org/10.1016/j.combustflame.2015.10.031.

[98] Howard JB, Essenhigh RH. The Mechanisms of Ignition of Pulverized Coal.

Combust Flame 1965;9:337–9.

[99] Mermoud F, Salvador S, Van de Steene L, Golfier F. Influence of the pyrolysis heating rate on the steam gasification rate of large wood char particles. Fuel 2006;85:1473–82. https://doi.org/10.1016/j.fuel.2005.12.004.

APPENDICES

A. Interface of the Software Used

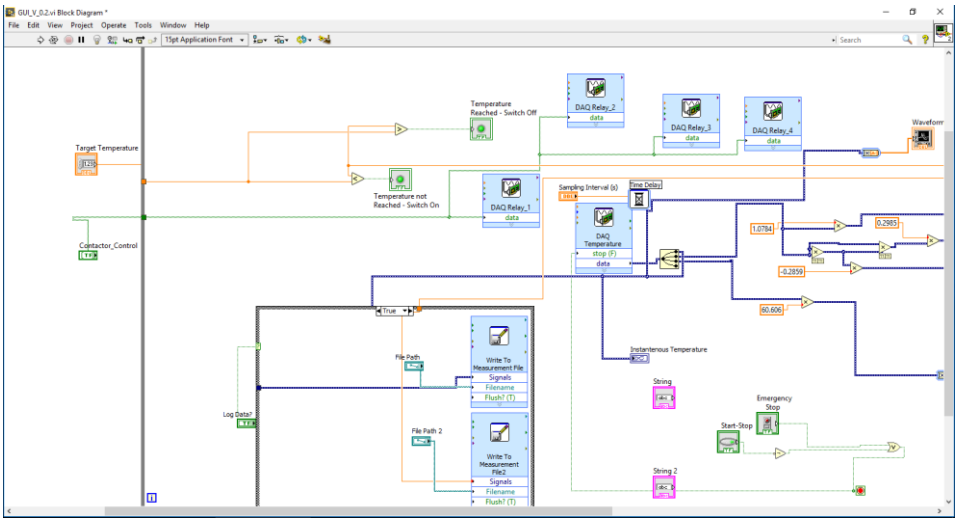

Figure 5.1 Schematic of the used LabVIEW code, part 1

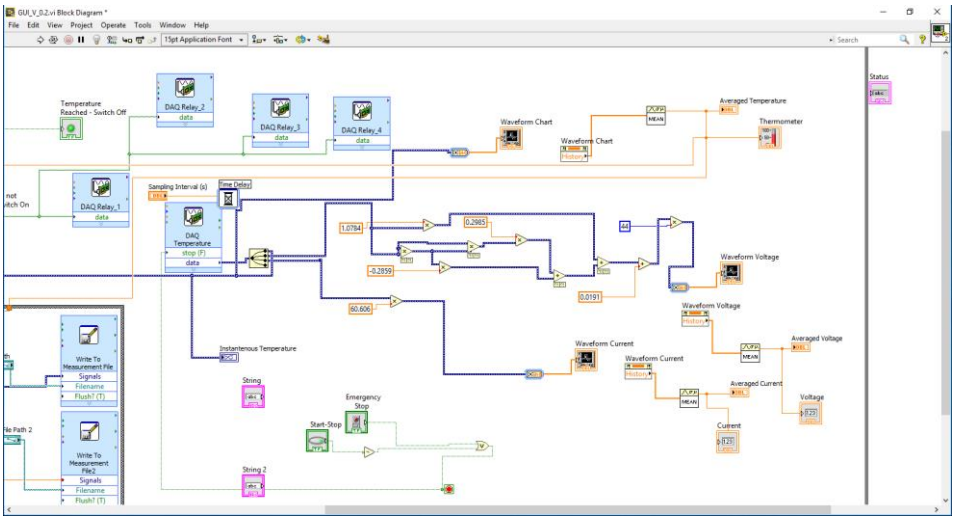

Figure 5.2 Schematic of the used LabVIEW code, part 2

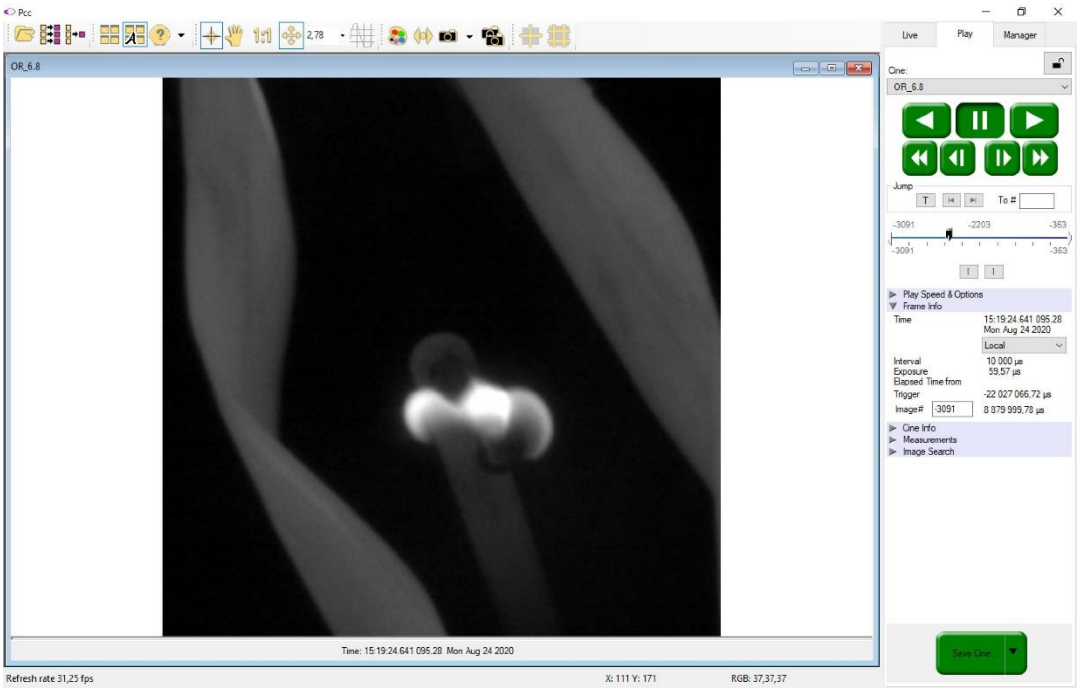

Figure 5.3 PCC Interface

B. Matlab Code

```
  clc
    clear all
    imgPath = '../../Desktop/ynei/';
    imgType = '*.tif'; % change based on image type
    images  = dir([imgPath imgType]);
    N = length(images);

    % check images
    if( ~exist(imgPath, 'dir') || N<1 )
        display('Directory not found or no matching images
found.');
    else
    % preallocate cell
    Seq{N,1} = [];
    for idx = 1:N
        Seq{idx} = imread([imgPath images(N-idx+1).name]);
    end
    end
%     show=input('Which picture you want to look for start? \n');
%     imshow(Seq{show});
    show2=input('Which picture you want to look for core? \n');
    imshow(Seq{show2});
    x=input('What is the x coordinate for start? \n');
    y=input('What is the y coordinate for start? \n');
    xst=input('What is the x start coordinate for core? \n');
    xend=input('What is the x end coordinate for core? \n');
    yst=input('What is the y start coordinate for core? \n');
    yend=input('What is the y end coordinate for core? \n');
%     for i=30:N
%         if (Seq{i}(x,y) -  Seq{i-1}(x,y)) <= 1
%             imshow(Seq{i})
%             start2=i;
%             break
%         end
%     end
    mesh=zeros(1,N);
    transpose(mesh);
    for i=1:N
        mesh(i)=Seq{i}(x,y);
    end
    avr=zeros(1,N);
    for k=1:N
        values=Seq{k}(xst:xend , yst:yend);
        meanv=mean(values);
        avr(k)=mean(meanv);
    end
    a=1:N;
    transpose(a);
```

```
   % plot(a,mesh);
    plot(a,avr);


    for k=200:N
       if avr(k+1) - avr(k) >= 30
           point1 = avr(k+1);
           lum1=k+1;
           fprintf('Start of the volatile combustion is point %d
with %.1f luminosity \n', lum1, point1);
           break
       end
    end
    difference=input('Difference between max and end? \n');
       for k=lum1+10:N-1
       if max(avr) - avr(k) >= difference
           point2 = avr(k);
           lum2=k;
           fprintf('End of the volatile combustion is point %d with
%.1f luminosity \n', lum2, point2);
           break
       end
    end
```